Construction and Building Materials 530 (2026) 146628

Contents lists available at ScienceDirect

Construction and Building Materials

journal homepage: www.elsevier.com/locate/conbuildmat

Evaluating the durability and cyclic thermal performance of lime mortars with microencapsulated PCMs for sustainable energy solutions

Andrea Rubio-Aguinaga, Loucas Kyriakou, José María Fernández, Íñigo Navarro-Blasco, José Ignacio Álvarez *

MATCH Research Group, Department of Chemistry, School of Sciences, University of Navarra, Irunlarrea, 1, Pamplona 31008, Spain

ARTICLE INFO

Keywords:
Phase Change Materials (PCMs)
Lime mortar
Durability
Cyclability
Thermal efficiency

ABSTRACT

Phase change materials (PCMs) have emerged as promising additives for lime renders aimed at moderating indoor temperatures and reducing heating and cooling demand in retrofit applications, including Built Heritage. However, existing studies largely report durability as a macroscopic pass-fail outcome and emphasize initial thermal benefits, with limited evidence on whether thermal functionality is retained after severe environmental ageing. This study addresses this gap by combining durability assessment with an integrated evaluation of post-exposure changes in microstructure, mechanical performance, and, critically, the conservation of thermal behaviour and thermal cyclability. Twelve lime render formulations incorporating microencapsulated paraffin PCMs with melting temperatures of 18 and 24 °C at 5, 10 and 20% by weight of lime, with and without 20% metakaolin, were investigated. Specimens were subjected to natural weathering, freeze-thaw cycling and salt attack, followed by post-durability characterization of microstructure, compressive strength and thermal performance. Functional thermal stability after ageing was assessed through a thermal agreement metric that directly links durability exposure with the preservation of functional thermal behaviour, enabling evaluation of whether thermal performance is merely present initially or effectively retained over time. In parallel, the retention and cyclic stability of latent heat storage and release were evaluated at both material and laboratory envelope scales. The results showed, first, that metakaolin-containing mortars exhibited significantly enhanced durability, successfully withstanding freeze-thaw and salt attack, whereas formulations without metakaolin failed prematurely. Following durability exposure, these optimized formulations displayed a refined pore network and preserved or improved mechanical performance, with compressive strength increases of up to 460%. Regarding the preservation of thermal functionality, PCM-metakaolin formulations generally exceeded 90% thermal agreement and reached 100% in several cases, while maintaining stable heat storage and release under repeated cycling. Overall, the results demonstrate that, when appropriately formulated, PCM-lime renders can combine durability with persistent and cyclable thermal performance, supporting their feasibility as long-lasting solutions for energy-efficient rehabilitation.

1. Introduction

The building sector is a major contributor to global energy consumption and emissions [1–4]. In 2021, buildings accounted for 34% of global final energy demand and 37% of energy- and process-related CO_2 emissions, underscoring the crucial role of building envelopes and materials to climate mitigation [1]. In Europe, the challenge is intensified by an aging building stock: more than 220 million building units, about 85% of the EU total, were built before 2001, and between 85% and 95% of today's buildings are expected to remain in use by 2050 [2]. Accordingly, the EU's policy framework aims for a fully decarbonised building stock by 2050, with deep renovation pathways designed to transform buildings into zero-emission ones after 2030 [2–4]. Given that a substantial proportion of the existing building stock will remain operational for several decades, and that rehabilitation generally entails a significantly lower environmental burden than demolition followed by new construction [5–7], retrofitting will play a decisive role in reducing the sector's carbon footprint [2,4,8,9]. It is therefore essential to identify construction materials that are both sustainable in production and capable of delivering enhanced energy efficiency with reliable long-term

* Correspondence to: Departamento de Química, Facultad de Ciencias, Universidad de Navarra, C/ Irunlarrea, 1, Pamplona, Navarra 31008, Spain.
E-mail address: jalvarez@unav.es (J.I. Álvarez).

https://doi.org/10.1016/j.conbuildmat.2026.146628
Received 24 February 2026; Received in revised form 15 April 2026; Accepted 6 May 2026

performance. This agenda aligns closely with the United Nations Sustainable Development Goals, specifically SDG 7 (Affordable and Clean Energy), SDG 11 (Sustainable Cities and Communities), and SDG 13 (Climate Action), which together emphasise reducing energy demand, preserving existing builds, and mitigating climate impacts [10].

Within this context, lime mortars have re-emerged as sustainable binders for both heritage conservation and low-impact construction [11–17]. Compared with ordinary Portland cement (OPC) mortars, air-lime systems exhibit lower embodied energy and CO_2 emissions at manufacture [16,18], while remaining chemically compatible with historic substrates and maintaining high vapour permeability, thus preventing moisture-related pathologies [15]. Crucially, lime mortars reabsorb CO_2 through carbonation during service life, partially offsetting process emissions [11–14]. This capacity for long-term carbon sequestration positions lime mortars as dynamic carbon sinks, reinforcing their relevance in sustainable construction strategies.

Despite these advantages, lime mortars exhibit limited thermal performance under operational conditions. Their low thermal inertia constrains the ability to stabilize indoor environments and reduce peak heating and cooling demands, especially in regions with large diurnal temperature variations [19,20]. This shortcoming is well-documented and remains a key obstacle when assessing lime mortars against contemporary energy-performance requirements. To address this, recent research has explored the incorporation of phase change materials (PCMs) [17,21–25]. PCMs undergo reversible phase transitions that enable them to absorb and release significant amounts of thermal energy within a defined temperature range [22,26,27]. When integrated into lime mortars, they provide latent heat storage and release, complementing the material's inherent sustainability. Several laboratory and pilot-scale studies have demonstrated that PCM-enhanced mortars can reduce indoor temperature fluctuations and lower heating and cooling loads, thereby improving the energy efficiency and thermal comfort [20–22,28,29].

Enhancing the energy efficiency of buildings largely depends on improving the thermal performance of the envelope, and renders represent a practical intervention layer [30–32]. In heritage contexts, where invasive retrofitting is not permissible, lime-based renders are especially valuable due to their chemical and physical compatibility with historic substrates and their ability to preserve permeability, essential for the conservation of traditional masonry [15,33]. Consequently, lime renders provide a suitable matrix for PCM incorporation [34].

Various strategies have been developed for incorporating PCMs into mortars, though their effectiveness varies widely. Direct incorporation into the binder is straightforward but presents major challenges, such as leakage during phase transitions, incompatibility with the alkaline matrix, and poor distribution heterogeneity [35,36]. Macroencapsulation, typically achieved by embedding PCMs in tubes, panels, or large capsules, reduces leakage but constitutes an invasive modification [36–38]. This approach is generally incompatible with heritage applications, as it does not comply with conservation requirements for minimally intrusive interventions [33]. In contrast, microencapsulation has proven to be the most effective and compatible solution [21,22,27,34]. Encapsulating PCMs within fine polymeric shells ensures homogeneous dispersion in the mortar, prevents leakage, stabilises PCM movement, and enhances heat-transfer for latent heat exchange [38]. Recent studies consistently highlight microencapsulation as the most reliable pathway for integrating PCMs into lime-based renders for both modern and heritage applications [21,22,27].

While improved thermal efficiency is critical, it alone does not guarantee sustainability [17,39,40]. If a material deteriorates rapidly, the environmental gains achieved during production and operation are neglected by the need for premature repair, replacement, or reinforcement, increasing life-cycle impacts [17,39,40]. Durability therefore becomes a central pillar of sustainable building envelopes, equally important as low embodied carbon and enhanced thermal performance. In this context, durability must be understood not only as resistance to physical degradation, but also as the capacity of the material to preserve its functional properties after exposure to environmental stressors. For PCM-enhanced mortars, long-term sustainability requires maintaining structural integrity, mechanical performance, and thermal functionality under environmental exposures and ensuring stable thermal performance under repeated cycles [41].

In conventional lime mortars, durability may be compromised by freeze-thaw cycling, salt crystallization, and combined climatic stresses [39,42]. These mechanisms progressively alter pore structure, induce cracking and scaling, and promote efflorescence, ultimately leading to loss of cohesion and material deterioration [39,42,43]. The incorporation of PCMs adds further complexity [34]: microencapsulated PCMs can potentially weaken mechanical strength if not properly integrated [22,44–46], and their inclusion can influence porosity and water absorption, key parameters governing resistance to environmental decay. Consequently, assessing durability in PCM-lime mortars requires a coupled evaluation of environmental resistance and post-exposure evolution of microstructural, mechanical and thermal properties.

Beyond these durability concerns lies another critical yet often overlooked aspect: the thermal cycling stability of PCMs within the mortar matrix. Since PCMs operate through repeated phase transitions, their long-term effectiveness depends on maintaining thermal storage and release capacity after numerous heating and cooling cycles [41]. A decline in latent heat capacity over time could significantly compromise energy efficiency of PCM-enhanced mortars. While previous studies have assessed the thermal behaviour of PCMs in controlled environments [21,47,48], limited research has evaluated their stability after understanding of how continuous phase change cycles affect their stability when embedded in lime mortars. Moreover, evaluating cyclability requires not only differential scanning calorimetry (DSC) analysis of phase transition enthalpies but also lab-scale energy performance tests under realistic conditions. In this study, both approaches are combined to provide a comprehensive assessment of the long-term viability of PCMs in lime-based mortars. This dual methodology enables a more accurate evaluation of whether PCM-enhanced mortars can sustain their energy-saving performance throughout service life, reinforcing their potential as sustainable construction materials.

Ultimately, the sustainability of PCM-lime renders must be assessed along three complementary axes: (i) conventional durability, defined as the ability of the material to preserve its physical integrity under aggressive environmental exposures such as freeze-thaw cycling, salt crystallization, and weathering; (ii) post-durability performance, encompassing the evolution of microstructure, mechanical resistance, and thermal behaviour following such exposures; and (iii) thermal cyclability, defined as the retention of latent-heat storage and temperature-damping capacity after repeated heating and cooling cycles. If either dimension fails, the anticipated benefits, in terms of reduced energy demand and improved comfort, are offset by maintenance or performance loss, undermining environmental gains. This systems perspective is consistent with broader sustainability and decarbonization frameworks, which emphasize durability and long-term performance alongside low embodied impact [1,2,4,10].

This study addresses a critical gap in the literature by examining both the durability under aggressive environmental exposures, understood not only as resistance to degradation but also as the post-durability evolution of microstructure, mechanical performance, and thermal behaviour, and the thermal cycling stability of lime mortars incorporating microencapsulated PCMs. While previous research has focused primarily on thermal benefits [21,23,29,49,50], this work explicitly investigates the resistance of PCM-enhanced lime mortars to environmental stressors and accelerated ageing, together with their post-exposure microstructural, mechanical, and thermal response, evaluating whether these materials remain structurally sound and thermally functional after exposure to weathering, freeze-thaw cycles, and salt crystallization, as well as their capacity to retain efficiency after

multiple phase-change cycles. The findings aim to determine whether PCM-enhanced lime mortars can provide a sustainable and durable solution for contemporary construction, contributing simultaneously to energy savings and the long-term preservation of built heritage.

2. Materials and methods

2.1. Materials

Rendering mortars were produced with CL-90-S hydrated calcitic lime (average particle size 10 μm, <10% >50 μm) sourced from Cal Industrial S.A. in Navarra and a calcareous sand (particle size 0–1 mm) from CTH (Huarte, Navarra, Spain), at a binder-to-aggregate ratio of 21.7/78.3 by weight. The water content was fixed at 25 wt% for all mixes. Raw materials were characterised by X-ray fluorescence (XRF) and X-ray diffraction (XRD) to determine their composition. XRF was performed with a Bruker S2 Puma apparatus and quantified using Spectra Results Manager software. The hydrated lime comprised: 96.54% CaO, 1.29% SO_3, 0.91% MgO, and 0.82% SiO_2. XRD identified portlandite ($Ca(OH)_2$) and calcite ($CaCO_3$) as the primary crystalline phases. The sand comprised of 94.61% CaO, 2.27% SiO_2, 0.79% Al_2O_3, and 0.73% MgO; XRD indicated calcite, quartz, montmorillonite, and hydrobiotite.

To optimize the fresh and hardened performance of the end-products, chemical additives and metakaolin (MK) were incorporated. Polycarboxylated ether derivative (MasterCast GT 205, Master Builders Solutions España S.L.U., Barcelona, Spain) was used as superplasticizer (SP), while a potato starch derivative (Casaplast KO09, Nova Casanova, Barcelona, Spain) acted as an adhesion booster. Metakaolin (Metaver N, NEWCHEM, Austria) was incorporated at 20% by weight of lime (bwol) in selected mixes to enhance strength and durability. XRF analysis of MK indicated a composition of 49.32% Al_2O_3 and 45.40% SiO_2 as the main constituents.

Two microencapsulated paraffin-based PCMs with melamine shells at different melting points (24°C for PCM24 and 18°C for PCM18) were added in mortars at 5%, 10%, and 20% bwol. A total of 14 mortar formulations were produced, including two PCM-free control mixes (Table 1). The adhesion booster was fixed at 0.50% bwol in all mixes. LM_0 contained SP at 0.60% bwol; all other renders contained SP at 0.75% bwol. The nomenclature for PCM-bearing renders follows a structured format: it begins with "LM" (Lime Mortar), followed by "P24" or "P18" to indicate the type of PCM incorporated (PCM24 or PCM18, respectively), and a subscript denoting the PCM content (% bwol). If metakaolin (MK) is present, it is indicated at the end as "MK" with its respective percentage in subscript.

2.2. Mortar preparation

The rendering mortars were prepared by mixing the dry components: air lime, calcareous sand, metakaolin (when applicable), microencapsulated PCMs, and the adhesion booster, in a BL-8-CA solid additive mixer (Lleal, S.A., Granollers, Spain) for 5 min to ensure homogeneity.

Water (25 wt%) was then added while mixing at low speed for 270 s in a Proeti ETI 26.0072 mixer (Proeti, Madrid, Spain). The superplasticizer (SP) was introduced progressively, following the dosages specified in Section 2.1, to optimize workability.

Fresh mortars were cast into moulds according to the target tests: cylinders (30 mm in diameter, 40 mm in height) for durability assessments, and rectangular panels (9 × 18 cm, 2 cm thick) for hotbox testing of thermal efficiency and phase change stability under cyclic heating and cooling conditions.

All specimens were cured under controlled laboratory conditions at 20 ± 0.5°C and 60% ± 5% relative humidity to ensure consistency across all tests.

2.3. Durability assessment

Long-term durability was evaluated through accelerated and extreme-exposure tests as follows:

(a)Weathering: Specimens were exposed to natural outdoor conditions for seven months, from April to November, in Pamplona, Navarra, Spain, located in the northern Iberian Peninsula within a climatic transition zone between Atlantic and Mediterranean regimes [51]. Over this period, mortars experienced minimum temperatures down to 2 °C in early spring, summer heat peaks approaching 39 °C, several heavy rainfall events exceeding 40 mm/day, and wind gusts above 80 km/h (Open-Meteo Historical Weather API). These conditions imposed combined thermal, moisture-related and mechanical stresses representative of environmental loads commonly encountered in mid-latitude European regions.

(b)Freeze-thaw cycles: Specimens were subjected to 28 two-stage cycles. Each cycle consisted of immersion in water at room temperature for 24 h followed by freezing at −20°C for 24 h in a Samsung RZ80FJSW freezer. The cycles were repeated up to 28 times or until complete degradation of the samples occurred. This procedure was adapted from EN 1367–1, which defines standardized methods for assessing resistance to freezing-thawing cycles [52].

(c)Salt attack: Specimens were fully immersed in a saturated aqueous $MgSO_4$ solution at 20°C and 95% relative humidity (RH) for 24 h, followed by oven drying at 110°C for 24 h. After every 10 cycles, the specimens were rinsed with water to remove residual salts. The procedure was repeated for up to 28 cycles or until complete disintegration of the samples. This protocol was adapted from EN 1367–2, which describes the magnesium sulfate test for evaluating resistance to salt crystallization processes [53].

Cylindrical specimens measuring 30 mm in diameter and 40 mm in height were used for all durability tests, with duplicates for each

Table 1
Mix design of lime-based mortars with varying PCM and metakaolin contents.

Mixture	Air lime (g)	Calcitic sand (g)	MK (g)	PCM24 (g)	PCM18 (g)	SP (g)	Adhesion booster (g)	Water/total solids
LM_0	217.0	783.0	-	-	-	1.3	1.1	0.25
LM_P24_5	217.0	783.0	-	10.9	-	1.6	1.1	0.25
LM_P24_{10}	217.0	783.0	-	21.7	-	1.6	1.1	0.25
LM_P24_{20}	217.0	783.0	-	43.4	-	1.6	1.1	0.25
LM_P18_5	217.0	783.0	-	-	10.9	1.6	1.1	0.25
LM_P18_{10}	217.0	783.0	-	-	21.7	1.6	1.1	0.25
LM_P18_{20}	217.0	783.0	-	-	43.4	1.6	1.1	0.25
LM_MK_{20}	217.0	783.0	43.4	-	-	1.6	1.1	0.25
$LM\_P24_5MK_{20}$	217.0	783.0	43.4	10.9	-	1.6	1.1	0.25
$LM\_P24_{10}MK_{20}$	217.0	783.0	43.4	21.7	-	1.6	1.1	0.25
$LM\_P24_{20}MK_{20}$	217.0	783.0	43.4	43.4	-	1.6	1.1	0.25
$LM\_P18_5MK_{20}$	217.0	783.0	43.4	-	10.9	1.6	1.1	0.25
$LM\_P18_{10}MK_{20}$	217.0	783.0	43.4	-	21.7	1.6	1.1	0.25
$LM\_P18_{20}MK_{20}$	217.0	783.0	43.4	-	43.4	1.6	1.1	0.25

condition (n = 2). Mass was recorded throughout the cycles to quantify weight loss or gain as an indicator of degradation. Additionally, the qualitative condition of the specimens was documented at each stage using a predefined damage scale (Table 2) previously established by the authors [22]. Representative images illustrating the progression of deterioration across the defined damage levels are presented in Fig. 1, complementing the scale provided in Table 2.

2.4. Post-durability characterization

Post-durability analyses were performed on cylindrical specimens that successfully withstood 28 cycles of freeze-thaw, salt attack, and weathering, together with an unaged reference sample, in order to assess potential alterations in composition, microstructure, mechanical performance and thermal behaviour.

A first set of analyses focused on pore structure, mechanical performance, and microstructural features. Pore structure was evaluated by mercury intrusion porosimetry (MIP) using a Micromeritics AutoPore IV 9500 porosimeter, operating within a pressure range of 0.0015–207 MPa. Measurements were performed on cubic fragments with an approximate edge length of 1 cm.

To complement the MIP results, scanning electron microscopy (SEM) was employed to directly observe microstructural features, phase distribution and damage patterns induced by the different ageing mechanisms. SEM analyses were performed using a COXEM EM-30N electron microscope equipped with secondary electron (SE) and backscattered electron (BSE) detectors. Elemental composition was determined by energy-dispersive X-ray spectroscopy (EDS) using a Quantax Compact30 system (Bruker), with data processed using Esprit Compact software. To ensure conductivity, samples were gold-coated using a COXEM SPT-20 ion sputter.

Mechanical performance was evaluated by compressive strength testing using a Frank/Controls 81565 press equipped with a Proeti ETI 26.0052 compressive breaking device. A controlled loading rate of 20–50 N/s was applied, with a loading duration between 30 and 90 s.

The thermal behaviour of the PCM-bearing renders after durability exposure was evaluated through controlled heating and cooling cycles in a climatic chamber (FCH-XENOLAB/1500). Surface temperatures were monitored using a FLUKE TiS55 + thermal camera. The cylindrical specimens described in Section 2.3 that survived all 28 durability cycles (freeze-thaw, salt attack, and weathering), together with an unaged reference, were subjected to a heating program from −10°C to 50°C. Thermal images were captured at 20, 30, and 50°C, followed by a cooling program from 50°C to −10°C, with images recorded at 30, 20, and −10 °C. At each temperature setpoint, qualitative colour mapping was used to visualise surface temperature distribution. In addition, a representative temperature value was extracted from the centre of each specimen to quantitatively monitor surface temperature evolution (Fig. 2).

Based on these measurements, the preservation of thermal behaviour after durability exposure (weathering, freeze-thaw and salt attack) was quantified through a thermal agreement percentage (%), introduced in this study as a performance-based indicator to directly assess the ability of the material to retain its original thermal response after ageing, rather than relying solely on absolute temperature values. This parameter enables a consistent comparison between formulations and exposure conditions by normalizing the response with respect to the intact specimen. Thermal agreement is defined by direct comparison between the surface temperature of the post-durability specimens and that of the intact (unaged) mortar under identical thermal setpoints. These setpoints were selected to cover both intermediate and extreme temperatures within the applied thermal cycles, ensuring a representative assessment of the material response under relevant thermal conditions.

Thermal agreement was calculated according to the following piecewise formulation:

$$\text{Thermal agreement}_i(\%) = \begin{cases} 100 \text{ if } \Delta T_i \le \tau \\ 100 \bullet \left(1 - \dfrac{\Delta T_i - \tau}{\Delta T_{max} - \tau}\right) \text{ if } \tau < \Delta T_i < \Delta T_{max} \\ 0 \text{ if } \Delta T_i \ge \Delta T_{max} \end{cases}$$

Where $\Delta T_i = \left| T_{unaged\ specimen,i} - T_{post-durability\ specimen,i} \right|$ represents the absolute surface temperature deviation between the intact (unaged) specimen and the specimen after durability exposure, measured at the same thermal setpoint. Here, τ represents the temperature deviation threshold beyond which differences relative to the unaged specimen are considered experimentally distinguishable. In this study, τ was set at 0.2 °C, corresponding to the resolution and experimental uncertainty associated with the thermal measurements. A maximum deviation ΔT_{max} of 5 °C was adopted; deviations equal to or greater than this value were considered indicative of severe alteration of thermal response, beyond which the material can no longer be considered to preserve its original functional behaviour, resulting in a thermal agreement of 0%. Specimens that did not successfully withstand the durability tests were directly assigned a thermal agreement value of 0%, as meaningful preservation of thermal behaviour could not be assumed.

This approach introduces a quantitative metric to evaluate the retention of functional thermal behaviour after durability exposure, providing a consistent basis for comparison between formulations and ageing scenarios. By normalizing the response with respect to the intact specimen, it enables a direct assessment of the extent to which the original thermal performance is preserved under different degradation conditions. This framework enables consistent comparison of the retention of thermal performance across formulations through evaluation at defined thermal states, while maintaining controlled and reproducible conditions.

Differential scanning calorimetry (DSC) was also performed to evaluate the retention of phase-change functionality in specimens that weathering, freeze-thaw and salt-attack exposure. Measurements were conducted using a DSC25 apparatus (TA Instruments), applying three heating and cooling cycles between −10 °C and 50 °C at a rate of 5 °C/min. Approximately 20 mg of powdered material, obtained by homogenizing fragments collected from different regions of the specimen after ageing exposure, was placed in 40 μL aluminium crucibles. Analyses were carried out under a nitrogen atmosphere (50 mL/min flow rate; 400 mL/min purge). The melting (ΔH_m) and crystallization (ΔH_c) enthalpies were determined and compared with those of the unaged specimens to identify potential changes in latent heat storage and release capacity following ageing exposure.

Table 2
Damage scale and visual assessment of durability tests.

Damage scale (0–10)	Characteristics
0	No visible damage; specimen intact.
1	Minimal material loss; almost no damage.
2	Small cracks; slight material loss.
3	Moderate cracks; visible wear.
4	Larger cracks; significant material loss.
5	Major cracks; pronounced material loss.
6	Severe cracks; surface starting to break apart.
7	Large sections missing; extensive cracking.
8	Structure heavily compromised; crumbling.
9	Near total destruction; disintegration visible.
10	Total destruction; specimen turned to dust.

2.5. Cyclic thermal performance

The cyclic thermal behaviour of PCM-bearing renders is a key indicator of their long-lasting sustainability. Ensuring that the PCMs maintain stable heat storage and release capacities throughout their service life is essential to confirm that no degradation or loss of effectiveness

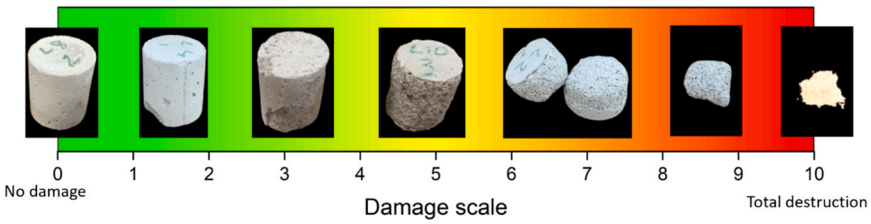

Fig. 1. Representative specimens at different levels of the damage scale, illustrating the progression from intact to severely deteriorated conditions during the durability tests.

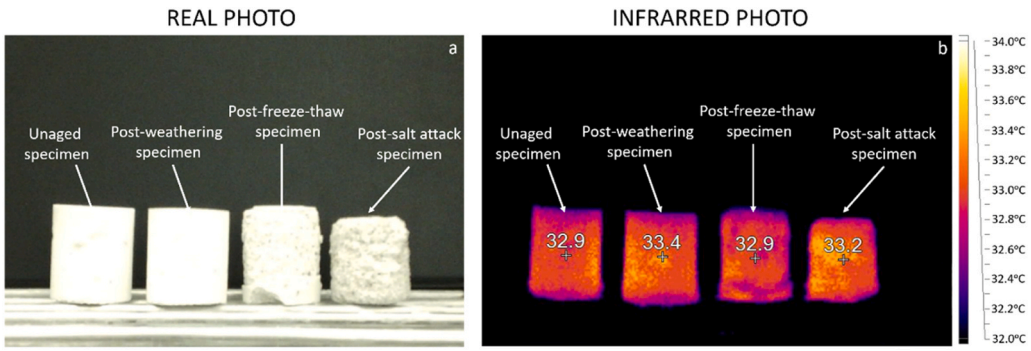

Fig. 2. Representative visual (a) and thermographic (b) images of lime-based mortar specimens before and after durability exposures.

occurs over time. To assess this performance, two complementary tests were conducted: differential scanning calorimetry (DSC) cyclic tests and hotbox cyclic tests.

DSC cyclic tests: Forty consecutive heating and cooling cycles were applied between −10°C and 50°C at a rate of 20 °C/min, which allows the observation of phase-change behaviour over a high number of consecutive cycles. Isothermal steps were included at the start and end of each cycle to ensure complete phase transitions, thereby improving accuracy and minimizing residual thermal effects [54,55]. The measurements were performed using a DSC25 apparatus with 40 μL aluminium crucibles. Each sample, approximately 20 mg, consisted of small fragments extracted from monolithic specimens to preserve their structural integrity. Analyses were carried out under nitrogen atmosphere with a flow rate of 50 mL/min and a nitrogen purge gas of approximately 400 mL/min. The enthalpy associated with melting (ΔH_m) and crystallization (ΔH_c) was recorded and monitored across the 40 cycles to identify any variations indicative of thermal fatigue or degradation.

To statistically evaluate the cyclic thermal behaviour of PCM-bearing renders and to provide robust insights into their reliability and long-term performance, descriptive analyses were performed using Microsoft Excel with the Real Statistics Resource Pack add-in. For each sample, the following parameters were computed across the 40 measurements: mean ($\bar{x}$), representing the average value [56]; median, reflecting the central tendency and robustness against outliers; standard Deviation (SD), quantifying data dispersion around the mean [56]; average absolute deviation (AAD), expressing the mean of absolute deviations from the average and offering a less outlier-sensitive measure [56]; and range, denoting the difference between maximum and minimum values [56]. Together, these descriptors provide a comprehensive evaluation of the PCM's enthalpy of melting and crystallization over repeated cycles, serving as indicators of long-term stability.

Hotbox cyclic tests: The cyclic thermal efficiency of PCM-bearing mortars was further evaluated using hotbox experiments, based on setups described in prior studies [21,22]. The hotbox simulates real building envelope conditions by exposing mortar slabs to alternating hot and cold environments under controlled boundaries. The tests were conducted on a representative subset of formulations, selected to ensure that the results are indicative of the overall behaviour of the PCM-modified systems. Four flat mortar slabs (9 × 18 cm, 2 cm thick) were mounted within a thermally insulated box, sealed hermetically with high-temperature silicone to ensure that heat transfer occurred exclusively through the mortar surfaces (Fig. 3). A total of 40 thermal cycles, between −10 °C and 50 °C were applied, while temperature variations were monitored in both a reference hotbox (without PCM) and a PCM-containing hotbox. During testing, the temperature damping capacity during heating and cooling, as well as the relative exchanged energy, were analysed to quantify the material's thermal efficiency throughout the cycling period [21,22]. The relative exchanged energy (Q*) was calculated as the time integral of the temperature difference between the reference and the PCM hotboxes over time $[t_1, t_2]$, performed with OriginLab software, according to Eq. 1.

$$Q^* = \int_{t1}^{t2} \Delta T(t)dt \quad \text{(Eq. 1)}$$

This equation captures the dynamic thermal behaviour of the system by integrating the continuous temperature evolution over time, thereby providing a direct estimation of the energy exchange throughout the full heating-cooling cycle.

The same statistical analysis described for the DSC data was applied to the hotbox results. The same parameters (mean, median, SD, AAD, and range) were computed across the 40 cycles to assess consistency, reproducibility, and potential degradation trends during repeated thermal cycling. This parallel statistical treatment ensures methodological coherence and allows direct comparison between micro-scale (DSC measurements) and lab-scale (hotbox) behaviour, providing a comprehensive and quantitatively supported evaluation of the long-term thermal stability of PCM-bearing renders.

3. Results and discussion

3.1. Durability assessment

Ensuring the long-term performance of construction materials is fundamental to achieving true sustainability. An effective formulation must not only enable the compatible incorporation of PCMs into the

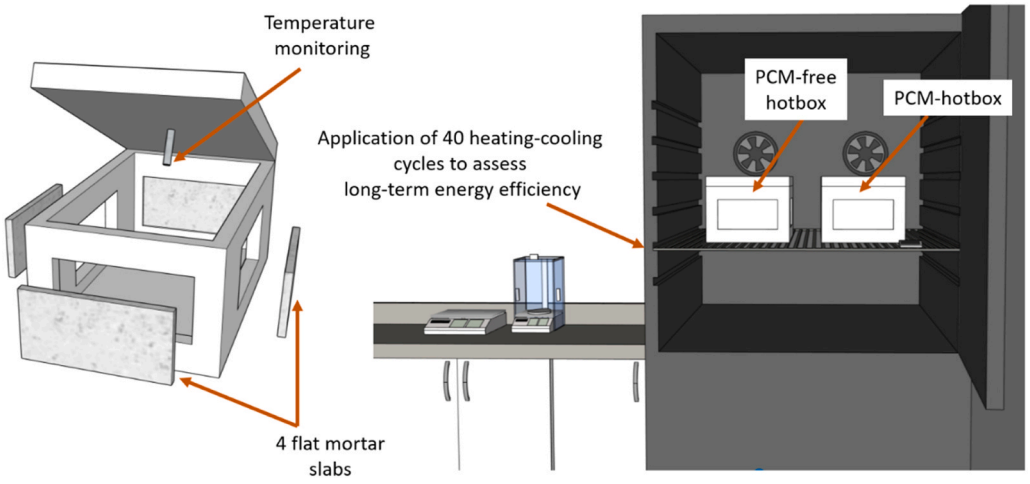

Fig. 3. Experimental hotbox setup for cyclic thermal performance evaluation of PCM-mortars.

mortar matrix while maintaining adequate fresh properties and workability but also enhance energy efficiency without compromising durability [34]. Optimizing the mix design is therefore essential to balance these aspects and produce materials capable of withstanding real-world environmental stressors over extended service lives. In this study, the mortar formulations were previously optimized to ensure full compatibility between lime and PCM, achieving satisfactory fresh, mechanical, and thermal performance as rendering mortars [34]. The present section evaluates whether these optimized formulations can also resist long-term durability challenges.

The freeze-thaw test results (Fig. 4a and Table 3) underscore the crucial role of metakaolin (MK) in enhancing durability. The reference mortars, LM_0 and LM_MK_{20}, showed markedly different behaviours: LM_0 failed catastrophically after only five cycles, whereas LM_MK_{20} completed all 28 cycles but exhibited significant deterioration (damage score = 9). This severe degradation of LM_0 is further corroborated by the pronounced mass loss observed during freeze-thaw cycling (Fig. 5a and Fig. 5b), which reflects the progressive disintegration of the specimens. These observations are consistent with previous studies [57–61], which attribute the improved resistance of MK-containing mortars to pozzolanic reactions, that densify the matrix and increase cohesion.

Notably, the most substantial improvement was observed in mortars combining both MK and PCMs, particularly $LM\_P24_{10}MK_{20}$, $LM\_P18_{20}MK_{20}$, and $LM\_P24_{20}MK_{20}$, which withstood 28 freeze-thaw cycles with only minor structural damage (damage score = 1–2). These formulations exhibited minimal mass variation throughout the test (Fig. 5a and Fig. 5b), indicating a high level of structural stability consistent with the limited visual damage observed. These results suggest that while MK enhances durability by strengthening the matrix, its synergy with PCMs further improves freeze-thaw resistance. This effect may be attributed to the PCMs' capacity to buffer internal temperature fluctuations, thereby reducing thermal stresses and mitigating microcracking during cyclic freezing and thawing [22,62–64]. Additionally, microencapsulated PCM particles constitute comparatively softer inclusions within the surrounding lime-MK matrix and can introduce new interfacial transition zones (ITZ) [21]. These locally more compliant regions within the microstructure could accommodate ice-induced expansion more effectively and thereby reduce stress concentrations during freezing.

In the salt attack test, a clear distinction emerged among the PCM-containing mortars (Fig. 4b and Table 3). While certain formulations with PCMs alone exhibited extensive deterioration similar to the reference mortars, those combining PCMs with metakaolin demonstrated markedly improved resistance. The reference mix LM_0 failed completely after 14 cycles (damage score = 10), whereas LM_MK_{20} completed all 28 cycles with a score of 7, showing notable degradation but improved performance relative to LM_0. This trend is mirrored by the evolution of specimen mass during sulfate exposure (Fig. 5c and Fig. 5d), where reference and PCM-only mortars experienced greater mass variation, indicative of material loss and surface degradation. In contrast, mortars incorporating both PCMs and MK, specifically $LM\_P24_{10}MK_{20}$, $LM\_P24_{20}MK_{20}$, $LM\_P18_{5}MK_{20}$, $LM\_P18_{10}MK_{20}$ and $LM\_P18_{20}MK_{20}$, consistently endured all 28 cycles with damage score of 6. Their comparatively stable mass throughout the test supports the visual assessment and confirms the enhanced resistance of these formulations to sulfate-induced deterioration (Fig. 5c and Fig. 5d). These findings indicate a clear synergistic effect between PCM and MK in enhancing resistance to salt-induced deterioration, thereby contributing to the preservation of structural integrity under chemically aggressive conditions. Considering that salt attack is particularly critical in coastal and saline environments [65,66], the superior performance of these optimized formulations highlights their potential for applications in such demanding exposure scenarios.

The enhanced durability of PCM-MK mortars can be attributed to the complementary roles of each additive. Metakaolin improves matrix cohesion through pozzolanic reactions that strengthen the binding phase and limit microcracking under external stresses [57–61]. In addition, the prolonged exposure to high moisture conditions during freeze-thaw and salt crystallization testing may have further promoted the progression of these pozzolanic reactions, as water availability enhances metakaolin reactivity compared to curing under ambient laboratory conditions [67], a mechanism further explored in Sections 3.2.1 and 3.2.2. In parallel, PCMs act as thermal buffers during freeze-thaw cycles, mitigating abrupt temperature variations and reducing the internal stresses associated with ice crystallization [22,62–64]. When combined, these effects produce a synergistic improvement in performance, with PCM-MK formulations exhibiting greater resistance than those containing either additive alone [22]. This synergy arises from the concurrent enhancement of matrix cohesion and moderation of thermal stresses, together reinforcing the long-term durability of lime-based mortars.

Table 4 complements Fig. 4 by presenting visual evidence of the damage sustained by the specimens during the durability tests. The images illustrate the progressive deterioration and highlight the differences in structural integrity among the various formulations. These visual records further substantiate the observed trends in freeze-thaw and salt attack resistance, which are consistently supported by the corresponding mass evolution data (Fig. 5), underscoring the protective and stabilizing role of PCM-MK combinations in lime mortars.

In addition to accelerated durability tests, natural weathering

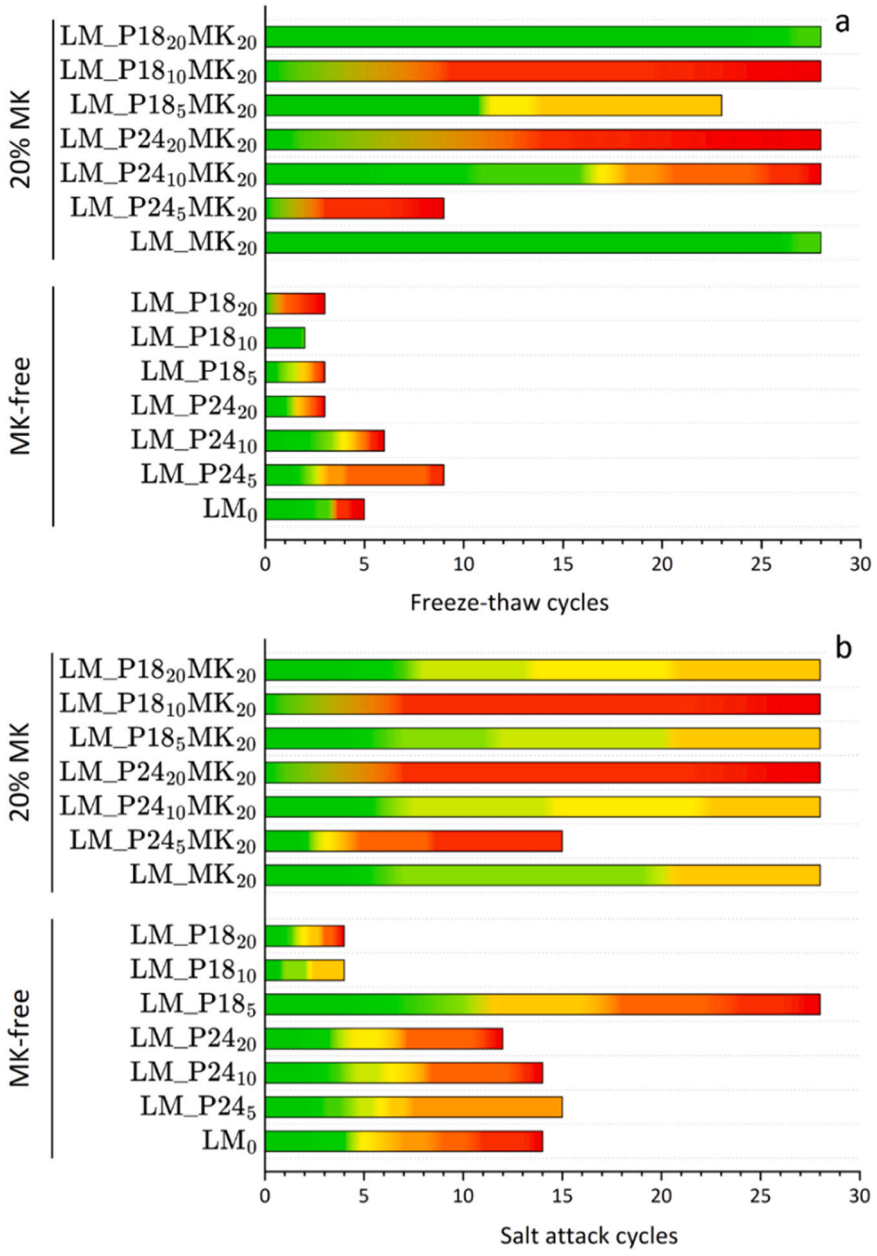

Fig. 4. Durability evaluation: damage scales for (a) freeze-thaw and (b) salt attack cycles.

Table 3
Cycles withstood and final damage scale of durability tests.

		Freeze-thaw		Salt attack	
	Mixture	Cycles withstood	Final damage scale (0–10)	Cycles withstood	Final damage scale (0–10)
MK-free	LM$_0$	5	10	14	10
	LM_P24$_5$	9	10	15	10
	LM_P24$_{10}$	6	10	14	10
	LM_P24$_{20}$	3	10	12	10
	LM_P18$_5$	3	10	28	9
	LM_P18$_{10}$	2	10	4	10
	LM_P18$_{20}$	3	10	4	10
	LM_MK$_{20}$	28	9	28	7
20% MK	LM_P24$_5$MK$_{20}$	9	10	15	10
	LM_P24$_{10}$MK$_{20}$	28	1	28	6
	LM_P24$_{20}$MK$_{20}$	28	1	28	6
	LM_P18$_5$MK$_{20}$	23	10	28	6
	LM_P18$_{10}$MK$_{20}$	28	6	28	6
	LM_P18$_{20}$MK$_{20}$	28	2	28	6

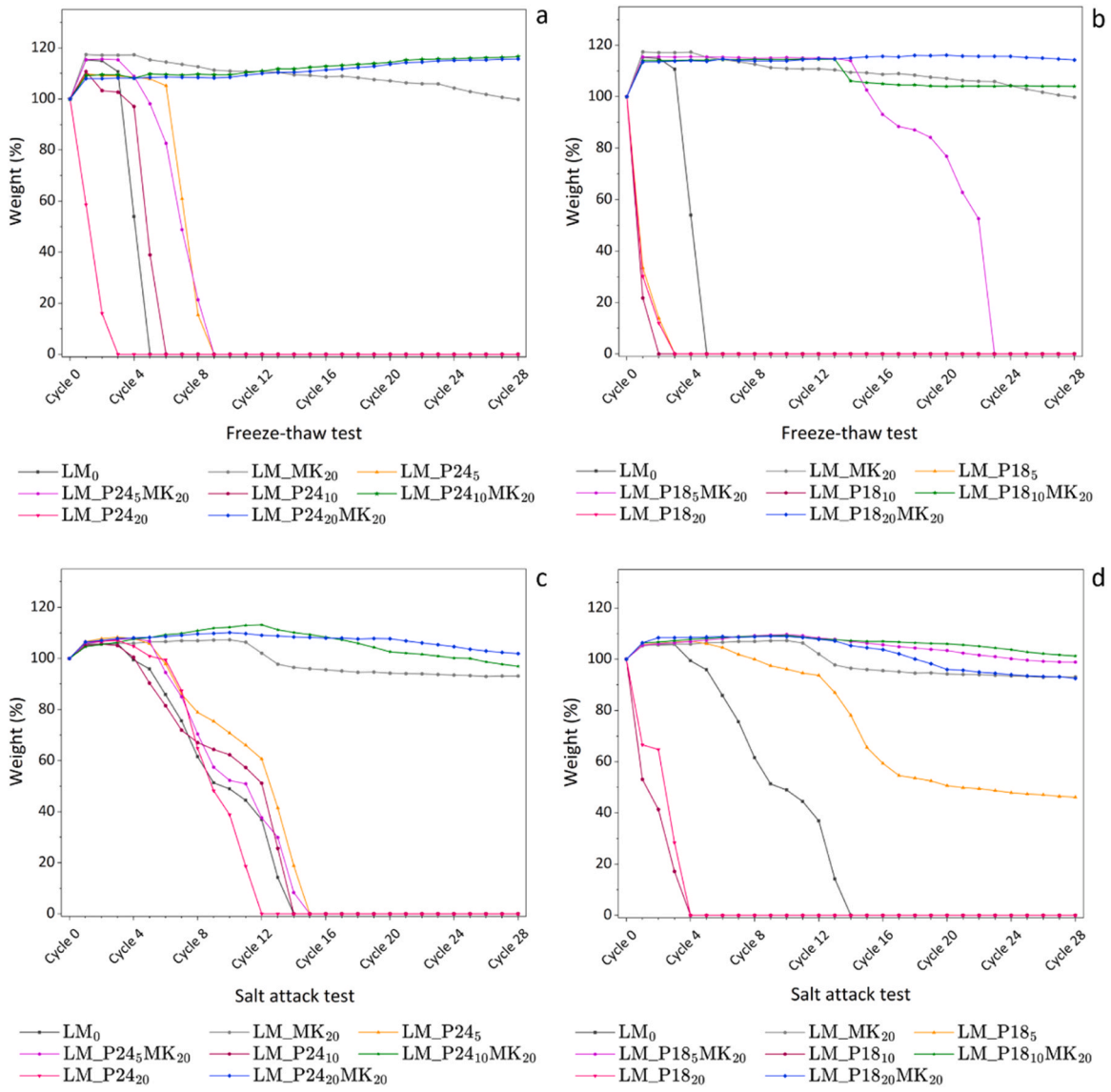

Fig. 5. Evolution of the average mass variation (%): a-b) Freeze-thaw cycles for references and PCM-modified mortars incorporating PCM24 and PCM18, respectively. (c-d) Salt attack cycles for references and PCM-modified mortars incorporating PCM24 and PCM18, respectively.

assessments further verified the long-term stability of the PCM-lime mortars (Table 5). After seven months of outdoor exposure, all samples remained structurally sound (Table 4), consistently exhibiting a damage level of 1. A slight weight increase of approximately 1% was recorded in all cases, attributed to ongoing carbonation [68] rather than moisture absorption, since the specimens were fully dried prior to weighing. These findings highlight the intrinsic stability of lime-based mortars under typical climatic conditions and confirm their suitability for durable, long-term applications.

The durability results position PCM-MK mortars as a significant advancement in sustainable construction materials. By combining high thermal efficiency with enhanced resistance to environmental degradation, these mortars extend structural service, thereby reducing maintenance requirements and material replacement frequency. This directly supports sustainability objectives, as improved durability minimizes resource consumption, waste generation, and energy use over time [10,40,69]. Rather than compromising durability, the incorporation of PCMs, particularly in synergy with metakaolin, strengthens the overall resilience of lime-based mortars, ensuring that gains in energy efficiency are not achieved at the expense of longevity. These materials thus offer an optimal balance between energy performance [21] and structural integrity, representing a durable and sustainable solution for resilient construction.

3.2. Post-durability microstructural and mechanical assessment

3.2.1. Microstructure evolution after durability exposure

Beyond the macroscopic assessment of durability based on visual integrity and mass variation, a comprehensive understanding of the long-term performance of lime-based mortars requires analysing how different ageing agents affect the internal pore network. Under real exposure conditions, durability-related degradation is often governed by microstructural changes that may not be necessarily visible at the specimen surface but progressively influence transport properties and internal stability [70]. In this context, mercury intrusion porosimetry (MIP) was employed to investigate the evolution of pore size distribution in a set of representative mortar formulations after the different durability tests. For each selected formulation, the unaged state was compared with the corresponding specimens subjected to weathered, freeze-thaw cycles and salt-attack (Fig. 6).

Regarding post-weathering microstructural analysis, the reference mortar containing metakaolin (LM_MK_{20}) exhibits a well-defined

Table 4
Comparative visual analysis of mortar specimens before and after exposure to weathering, freeze-thaw and salt attack cycles. Each individual sample is representative of the average state of all samples tested. The coloured rectangles in the bottom right corner indicate the damage level according to the scale defined in Table 2.

Damage scale (0-10)	Characteristics
0	No visible damage; specimen intact.
1	Minimal material loss; almost no damage.
2	Small cracks; slight material loss.
3	Moderate cracks; visible wear.
4	Larger cracks; significant material loss.
5	Major cracks; pronounced material loss.
6	Severe cracks; surface starting to break apart.
7	Large sections missing; extensive cracking.
8	Structure heavily compromised; crumbling.
9	Near total destruction; disintegration visible.
10	Total destruction; specimen turned to dust.

Mixture	Original state	Weathering	Freeze-thaw	Salt attack
LM_0	Cycle 0 (intact) 	After 6 months 	Failure at cycle 5 (total destruction) 	Failure at cycle 14 (total destruction) 
LM_P18_5	Cycle 0 (intact) 	After 6 months 	Failure at cycle 3 (total destruction) 	Cycle 28 (final) 
LM_MK_{20}	Cycle 0 (intact) 	After 6 months 	Cycle 28 (final) 	Cycle 28 (final) 
$LM\_P24_{20}MK_{20}$	Cycle 0 (intact) 	After 6 months 	Cycle 28 (final) 	Cycle 28 (final) 

Table 5
Evolution of specimen weight during natural weathering exposure.

Mixture	Initial weight (g)	Final weight (g)	Weight change (%)
LM_0	55.5	56.4	1.6
LM_P24_5	53.7	53.9	0.4
LM_P24_{10}	53.8	54.5	1.3
LM_P24_{20}	53.3	52.6	-1.3
LM_P18_5	64.0	64.2	0.3
LM_P18_{10}	53.6	55.2	3.0
LM_P18_{20}	54.0	54.6	1.1
LM_MK_{20}	58.3	59.3	1.7
$LM\_P24_5MK_{20}$	55.6	56.1	0.9
$LM\_P24_{10}MK_{20}$	54.4	55	1.1
$LM\_P24_{20}MK_{20}$	54.9	55.5	1.1
$LM\_P18_5MK_{20}$	66.4	67.5	1.7
$LM\_P18_{10}MK_{20}$	65.7	66.8	1.7
$LM\_P18_{20}MK_{20}$	65.2	66.1	1.4

capillary pore peak centred at approximately 0.68 μm in the unaged state. After natural weathering, this peak shifts towards a smaller pore diameter, around 0.55 μm, while the overall shape of the distribution remains narrow and well defined (Fig. 6a). This shift towards finer pore sizes is consistent with microstructural densification processes promoted under outdoor exposure, where prolonged availability of atmospheric CO_2 promotes carbonation of portlandite and precipitation of calcite within the capillary pore network [71–73]. In the presence of metakaolin, this effect is further reinforced by continued pozzolanic reactions consuming portlandite and forming C-S-H phases, thereby refining the capillary structure [74].

A similar trend is observed in PCM-bearing mortars incorporating metakaolin. In $LM\_P24_{10}MK_{20}$, the dominant pore diameter decreases from approximately 0.84 μm in the unaged state to about 0.68 μm after weathering (Fig. 6b). Likewise, in $LM\_P18_{20}MK_{20}$, the main capillary peak shifts from around 1.05 μm to approximately 0.68 μm following weathering exposure (Fig. 6f). In both formulations, the displacement is accompanied by a clear reduction in peak intensity, indicating redistribution of the accessible pore network. This behaviour can be attributed to the partial filling of capillary pores by carbonation products and progressive pozzolanic reaction development [71–74]. In other PCM-bearing mortars with metakaolin ($LM\_P24_{20}MK_{20}$ and $LM\_P18_5MK_{20}$), natural weathering does not induce a marked displacement of the dominant pore diameter. However, a consistent attenuation of the main capillary peak is observed relative to the unaged state (Fig. 6d-e). This systematic reduction in peak intensity suggests partial pore filling and densification, while preserving the characteristic pore size range defined by the initial microstructure. A similar behaviour is also observed in the PCM-bearing mortar without metakaolin (LM_P24_{20}), where natural weathering results in attenuation of the principal pore peak without significant positional displacement (Fig. 6c).

In contrast to natural weathering, freeze-thaw exposure induces a more demanding deterioration scenario in which only mortars incorporating metakaolin remain intact after cyclic freezing and thawing (Fig. 6). In these formulations, the pore size distributions reveal a systematic displacement of the dominant capillary pore peak towards smaller diameters. At the same time, the distributions remain coherent and well-defined with no evidence of pore coarsening or the emergence of larger pore domains (Fig. 6a, b, d, f). For example, in LM_MK_{20} the characteristic pore size shifts from approximately 0.68 μm in the unaged state to about 0.43 μm after freeze-thaw cycling, while in PCM-bearing MK mortars such as $LM\_P24_{20}MK_{20}$ the main peak moves from around 0.83 μm to approximately 0.68 μm. The absence of pore coarsening and preservation of the structured capillary network indicate that freeze-thaw cycling does not induce microcracking or internal cohesion loss in MK-containing mortars. Instead, the observed pore refinement suggests further matrix densification under repeated moisture saturation. The high water availability during freeze-thaw cycles promotes the progression of pozzolanic reactions [67], while limiting carbonation due to reduced CO_2 transport through water-filled pores [75,76]. Consequently, microstructural evolution under freeze-thaw conditions appears to be governed by reaction-driven pore refinement, rather than damage-induced pore enlargement. By contrast, PCM-bearing mortars without metakaolin did not withstand freeze-thaw cycling and experienced severe structural degradation leading to complete loss of specimen integrity (Fig. 4). The absence of post-exposure MIP data for these formulations reflects the extend of deterioration and highlights the critical role of formulation optimisation, particularly the incorporation of metakaolin, in stabilising the matrix under cyclic thermal and moisture stresses.

Salt attack induces more pronounced modifications in the pore size distributions compared to natural weathering and freeze-thaw exposure, particularly in terms of peak attenuation and redistribution of the pore network towards finer size ranges (Fig. 6). In all mortars that retained structural integrity after salt exposure, the post-attack curves display a substantial reduction in main capillary peak intensity, together with a shift of the characteristic pore diameter to smaller values (Fig. 6a, b, d-f). Moreover, salt-exposed specimens show an increased relative contribution of finer pores below 0.1 μm, especially in $LM\_P24_{20}MK_{20}$, $LM\_P18_5MK_{20}$ and $LM\_P18_{20}MK_{20}$ (Fig. 6d-f). This redistribution towards finer pores is consistent with a pore-filling mechanism associated with salt crystallization, where precipitation of salt crystals partially occupies capillary pores and modifies the accessible pore network [77, 78]. Importantly, no evidence of pore coarsening is detected in the formulations that withstand salt exposure, indicating that the microstructural modifications are governed by filling and redistribution processes rather than damage-driven pore enlargement.

Overall, the MIP results highlight the critical importance of formulation optimisation in controlling the durability of PCM-bearing lime mortars. The preservation of a coherent and refined pore network, even under aggressive ageing conditions such as freeze-thaw cycling and salt crystallization, demonstrates that appropriate matrix design is essential for maintaining microstructural stability. The synergistic incorporation of PCMs and metakaolin produces a pore structure capable of accommodating phase transitions, moisture fluctuations, and crystallization stresses without pore coarsening or structural disruption. This microstructural resilience provides strong evidence of enhanced durability and supports the expectation of extended service life for properly formulated PCM-bearing lime mortars incorporating metakaolin.

Beyond the quantitative pore structure analysis provided by MIP, scanning electron microscopy (SEM) was conducted to further evaluate the post-durability microstructure of the mortars, allowing direct examination of matrix continuity and the morphological integrity and dispersion of the microencapsulated PCM within the lime matrix.

SEM observations revealed a well-preserved microstructure after all durability exposures (Fig. 7). As shown in Fig. 7a-b (post-weathering), the lime-metakaolin matrix exhibits a compact and continuous morphology, without evident microcracking, matrix disruption or pore coarsening. The microencapsulated PCM particles remain clearly identifiable, maintaining their spherical geometry and appearing homogeneously distributed throughout the matrix. No signs of shell rupture, collapse or interfacial debonding are observed.

A similar behaviour is evident after freeze-thaw exposure (Fig. 7c-e). The matrix retains structural cohesion, and the microcapsules appear intact and uniformly embedded despite the cyclic volumetric stresses associated with repeated freezing and thawing. The absence of microstructural discontinuities is fully consistent with the preserved pore network characteristics identified by MIP (Fig. 6) and with the macroscopic integrity observed in the specimens after testing (Fig. 4).

Following salt crystallization (Fig. 7f), mortar microstructure likewise remains cohesive. The PCM microcapsules preserve their morphology and are well accommodated within the surrounding matrix, with no observable damage attributable to crystallization pressures. This

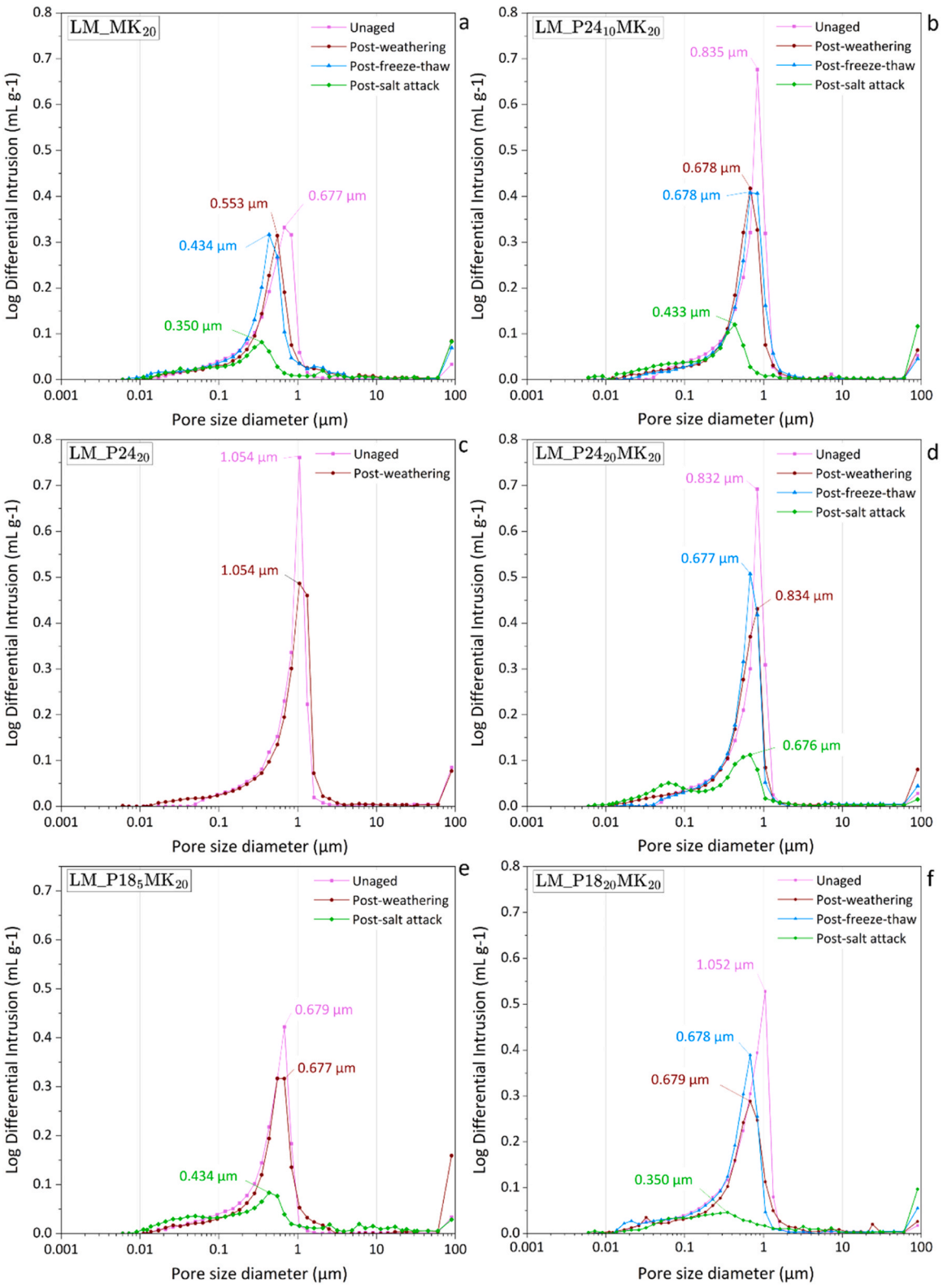

Fig. 6. MIP pore size distribution of selected lime-based mortars after durability exposure: (a) LM_MK$_{20}$, (b) LM_P24$_{10}$MK$_{20}$, (c) LM_P24$_{20}$, (d) LM_P24$_{20}$MK$_{20}$, (e) LM_P18$_{5}$MK$_{20}$ and (f) LM_P18$_{20}$MK$_{20}$. For each formulation, pore size distributions are shown for the unaged state and after natural weathering, freeze-thaw cycling and salt attack, where applicable. Missing curves correspond to specimens that did not withstand the respective durability test.

behaviour indicates that the system withstands not only cyclic thermal and moisture variations but also physicochemical stresses induced by salt growth within the pore structure.

Elemental mapping (Fig. 8) further confirms the stable integration of the microcapsules within the matrix. The carbon-rich domains corresponding to the PCM core are clearly distinguished in Fig. 8c, while calcium (Fig. 8d) is predominantly associated with the lime-base binder. Silicon and aluminium (Fig. 8e-f) are homogenously distributed within

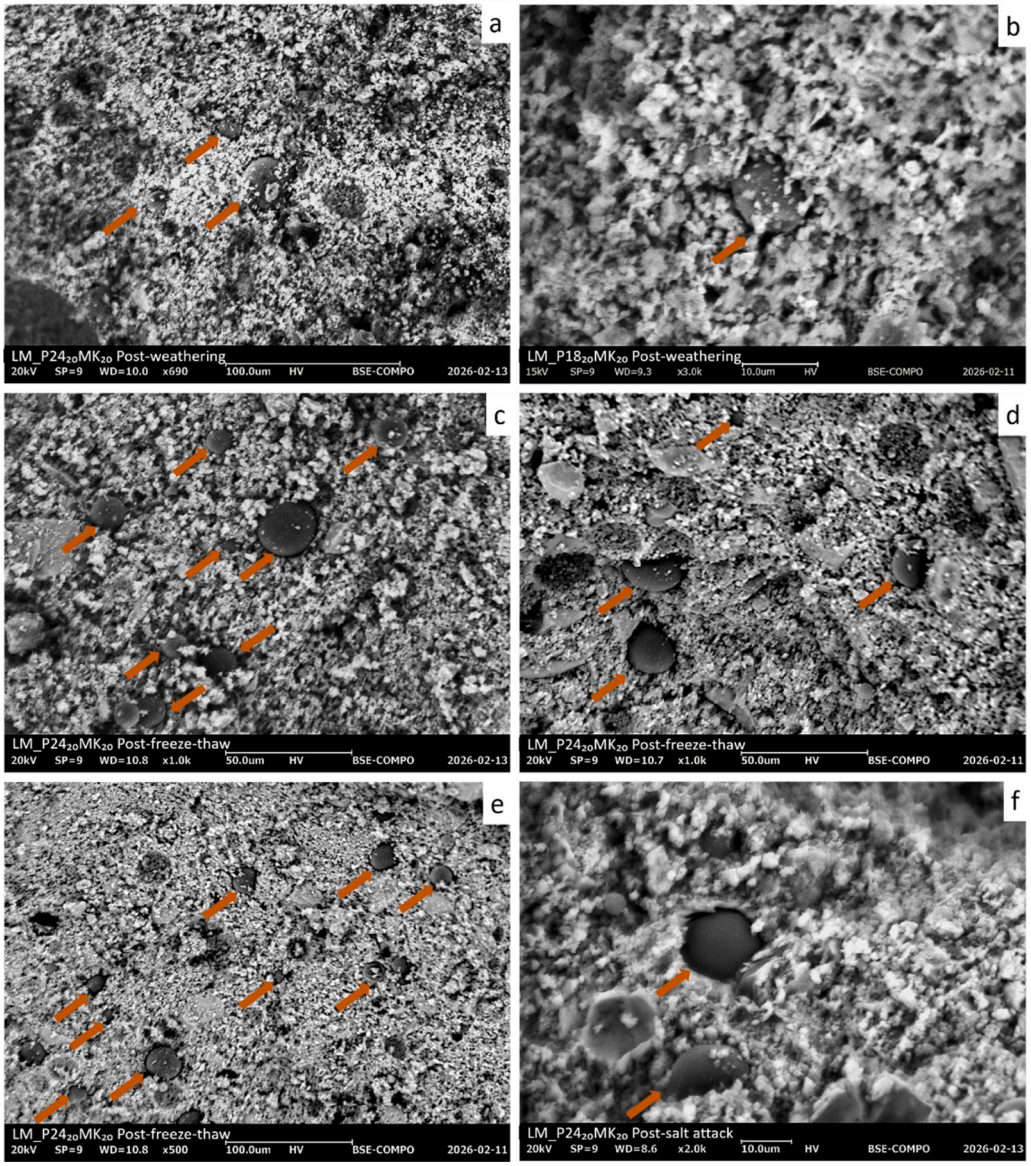

Fig. 7. SEM micrographs of PCM-lime mortars after durability exposure: (a-b) post-weathering, (c-e) post-freeze-thaw, and (f) post-salt crystallization. Orange arrows highlight the location of microencapsulated PCM particles.

the matrix, reflecting the contribution of metakaolin-derived phases. These results support the morphological observations, evidencing homogeneous PCM dispersion and strong matrix-capsule compatibility without mortar segregation or interfacial degradation.

Overall, SEM analysis demonstrates that durability exposure did not induce microstructural deterioration in either the binder matrix or the microencapsulated PCMs. The preserved matrix continuity likely contributes to protecting the microcapsules from mechanical and crystallization-related stresses, thereby maintaining their physical integrity. This microstructural stability provides a robust basis for the retention of thermal functionality, which is quantitatively assessed in Section 3.3.

3.2.2. *Post-durability mechanical properties*

Compressive strength results reveal a strong dependence of mechanical performance on both durability exposure and mortar formulation, particularly on the incorporation of metakaolin (Fig. 9). After natural weathering, all mortars exhibited increased compressive strength compared to their unaged state, regardless of PCM content. This systematic improvement confirms that outdoor exposure did not induce mechanical degradation but instead promoted matrix consolidation, in agreement with the MIP findings (Fig. 6). The effect was particularly pronounced in metakaolin-containing mortars: LM_MK$_{20}$ increased from 2.5 MPa to 6.5 MPa, while LM_P18$_5$MK$_{20}$ reached values up to 8.0 MPa. These gains are attributed to the combined progression of lime carbonation and continued pozzolanic reactions, which densify the microstructure and enhance interparticle bonding [68,70,79]. Increased moisture availability under weathering conditions likely further promoted pozzolanic activity involving metakaolin, contributing to matrix consolidation and strength development [67]. These results are consistent with the low damage scale values (Table 1Tables 3–4) and the pore refinement trends identified by MIP (Fig. 6).

A markedly different response was observed under freeze-thaw exposure. PCM-containing mortars without metakaolin did not withstand the full set of cycles and failed before test completion, resulting in compressive strength values of 0 MPa. The absence of a reinforced binding phase facilitated crack initiation and propagation under repeated ice formation pressures [80], ultimately leading to structural disintegration (Fig. 4a and Table 4)

In contrast, mortars incorporating both PCMs and metakaolin

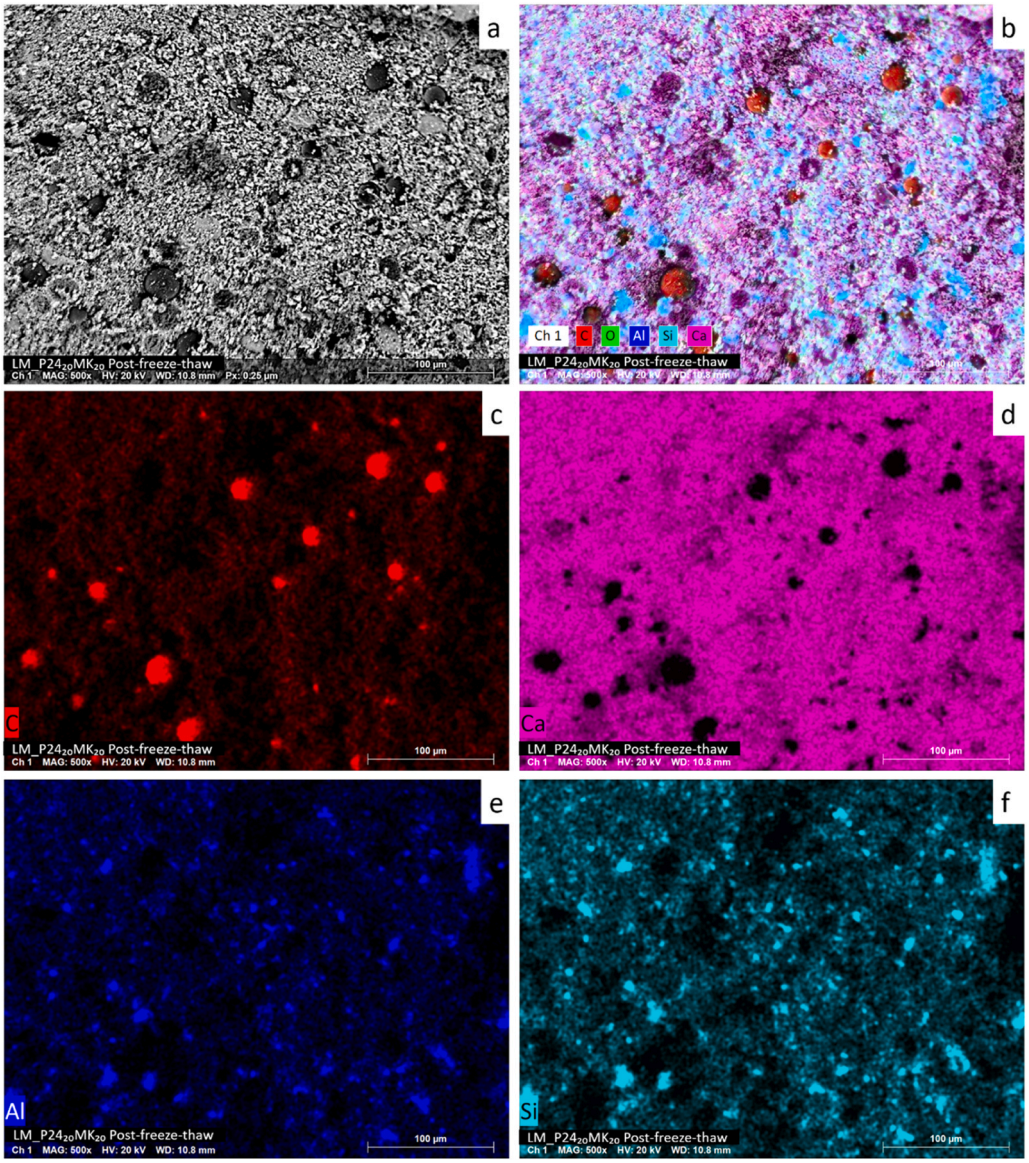

Fig. 8. SEM-EDS elemental mapping of PCM-lime mortar after freeze-thaw testing, illustrating matrix composition and PCM distribution: (a) SEM image, (b) composite map, (c) C, (d) Ca, (e) Al, and (f) Si mappings.

retained measurable compressive strength after freeze-thaw cycling and, in several cases, exhibited improvements relative to their unaged state, evidencing a substantially enhanced mechanical resilience (Fig. 9). For instance, LM_P18$_{10}$MK$_{20}$, increased from 2.5 MPa to 3.1 MPa (ca. 22%), and LM_P24$_{10}$MK$_{20}$ rose from 2.7 MPa to 3.6 MPa (ca. 33%). At higher PCM contents, the effect was more pronounced: LM_P24$_{20}$MK$_{20}$ increased from 4.0 MPa to 5.6 MPa (~40%).

This behaviour differs from that of LM_MK$_{20}$ (PCM-free MK-bearing reference mortar), in which compressive strength was largely preserved after freeze-thaw exposure but did not exceed unaged value. This distinction underscores the additional contribution of PCMs when incorporated within a reinforced lime matrix. The observed strength gains support the active role of PCMs in mitigating freeze-thaw-induced damage by attenuating internal thermal gradients and reducing cyclic freezing stresses [22,62–64]. When combined with the pore structure refinement and enhanced matrix cohesion provided by metakaolin [57–59,61], this thermal buffering is able not only to withstand freeze-thaw cycling but, in some cases, to further mechanical consolidation (Fig. 9). Moreover, repeated water exposure during freeze-thaw cycling likely promotes ongoing pozzolanic reactions [67], further reinforcing the lime matrix and contributing to the improved mechanical performance observed in MK-containing mortars. This interpretation is consistent with the low damage scale values, preserved specimen integrity after freeze-thaw testing (Fig. 4a), and the refined pore network identified by MIP analysis (Fig. 6).

A comparable formulation-dependent trend was observed after salt crystallization cycles. PCM-containing mortars without metakaolin again failed to complete the durability test, resulting in complete structural disintegration (Fig. 4b), with the exception of LM_P18$_5$, which did not undergo total destruction but exhibited severe damage. This collapse reflects the severe stresses generated by salt crystallization within a weakly reinforced lime matrix, leading to loss of cohesion and load-bearing capacity (Fig. 4b).

Mortars combining PCMs with metakaolin, however, retained significant compressive strength after salt exposure and, in several cases, clearly exceeded their unaged values (Fig. 9). For instance, LM_P24$_{10}$MK$_{20}$ increased from 2.7 MPa in the unaged state to 15.1 MPa after salt exposure (ca. 460%), while LM_P18$_{10}$MK$_{20}$ rose from 2.5 MPa to 12.5 MPa (ca. 400%). These substantial increases indicate that, at intermediate PCM contents, the synergistic interaction between PCMs

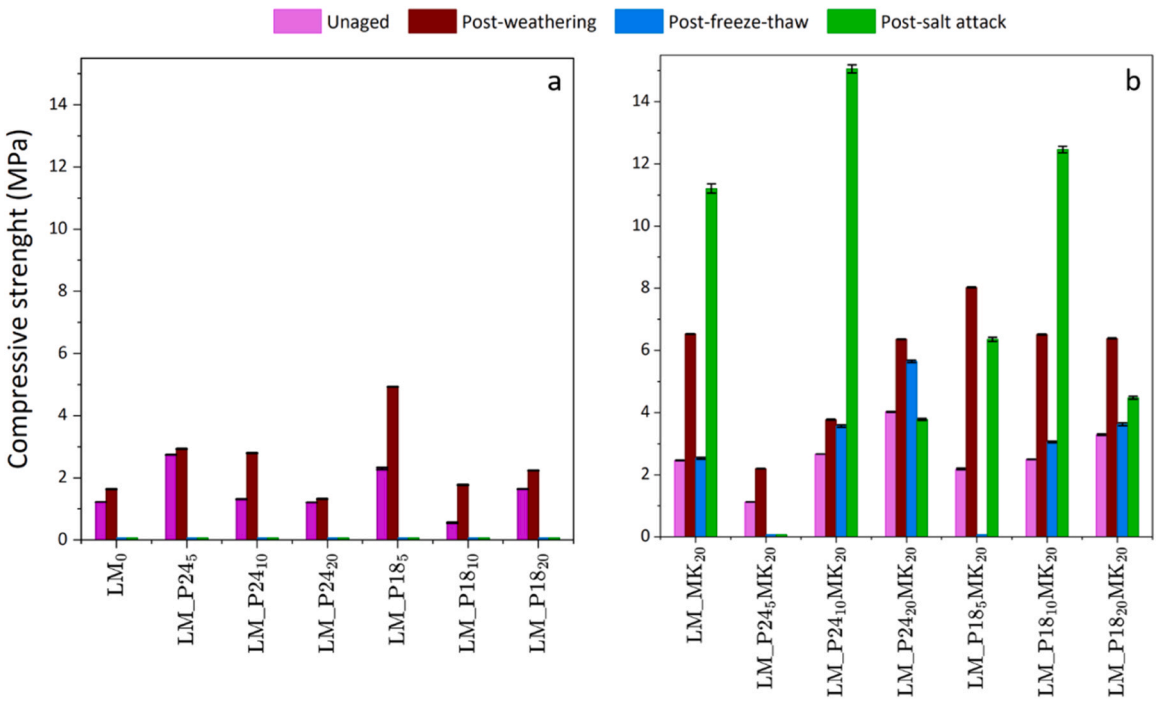

Fig. 9. Compressive strength of PCM-enhanced lime mortars before and after durability exposure: (a) formulations without metakaolin and (b) formulations with 20% bwol of metakaolin.

and metakaolin not only mitigates salt-induced damage but can also result in pronounced mechanical strengthening.

At higher PCM contents, the response became more formulation-sensitive. LM_P24$_{20}$MK$_{20}$ exhibited a compressive strength of 3.8 MPa after salt exposure, slightly below its unaged value of 4.0 MPa (ca. 6% reduction), whereas LM_P18$_{20}$MK$_{20}$ increased from 3.3 MPa to 4.5 MPa (ca. 36% increase). Despite these variations, all MK-containing PCM mortars retained measurable compressive strength after salt crystallization, in clear contrast to MK-free formulations, which failed to complete the test. Taken together, the observed mechanical response reflects not only resistance to degradation but also continued consolidation of the material under the combined effects of pore refinement, salt-induced pore filling and favourable moisture conditions for ongoing pozzolanic reactions.

Overall, these findings indicate that although salt crystallization generates severe internal stresses, the incorporation of metakaolin enables the lime matrix to accommodate such stresses effectively, thereby preserving structural integrity and, in many cases, enhancing mechanical performance (Fig. 9). This response is consistent with the lower damage scale values and reduced surface degradation observed in MK-containing mortars after salt exposure (Fig. 4), as well as with the refined pore structure evidenced by MIP analysis (Fig. 6).

Collectively, the results demonstrate that the mechanical durability of PCM-enhanced lime mortars is not an inherent consequence of PCM incorporation alone, but rather the outcome of a balanced and optimized formulation. When PCMs are combined with metakaolin, the mortars exhibit a pronounced capacity to withstand aggressive ageing conditions, retaining or even improving their compressive strength after freeze-thaw and salt crystallization exposure. This level of mechanical resilience confirms that PCM-MK formulations are not only functionally effective from a thermal perspective but also structurally robust over time. Such durability is fundamental to sustainability, as only mortars capable of maintaining mechanical integrity under realistic environmental stresses can be considered viable long-term solutions for building applications.

3.3. Post-durability thermal performance

3.3.1. Post-durability conservation of thermal behaviour

The thermal performance of PCM-bearing mortars before and after durability exposure was evaluated in terms of thermal agreement (%), using the intact (unaged) specimens as the functional reference. Rather than focusing on absolute surface temperatures, the analysis emphasised each formulation's capacity to preserve its original thermal response following severe environmental ageing. Representative thermographic images illustrating the heating and cooling stages are presented in Fig. 10, while the corresponding thermal agreement values used for quantitative comparison are summarised in Fig. 11.

During the heating stage (20, 30 and 50 °C), thermal agreement values reveal distinct differences in the ability of the mortars to retain their thermal behaviour after durability exposure (Fig. 11). Weathered specimens consistently exhibited high thermal agreement across all formulations, generally exceeding 90%. This indicates that prolonged outdoor exposure did not significantly alter the thermal response of either reference or PCM-modified mortars. This outcome is particularly relevant, as natural weathering represents the most realistic service condition for lime-based renders.

Following freeze-thaw cycling and salt attack, thermal agreement was strongly dependent on matrix composition. The reference mortar without metakaolin (LM$_0$) and MK-free PCM-bearing mortars consistently exhibited thermal agreement values of 0%, as these specimens did not withstand the full durability programme. Consequently, no preservation of thermal behaviour relative to the intact reference could be assumed for these formulations. In contrast, mortars incorporating metakaolin demonstrated outstanding preservation of thermal behaviour after both freeze-thaw and salt exposure. MK-containing formulations consistently exhibited high thermal agreement values during heating, frequently exceeding 90% and, in several cases, reaching 100% (Fig. 11). This response was observed for both PCM18- and PCM24-based systems and across different PCM dosages, indicating that the combined incorporation of PCMs and metakaolin enables the material not only to survive severe durability conditions structurally, but also to maintain a thermal response essentially identical to that of the intact

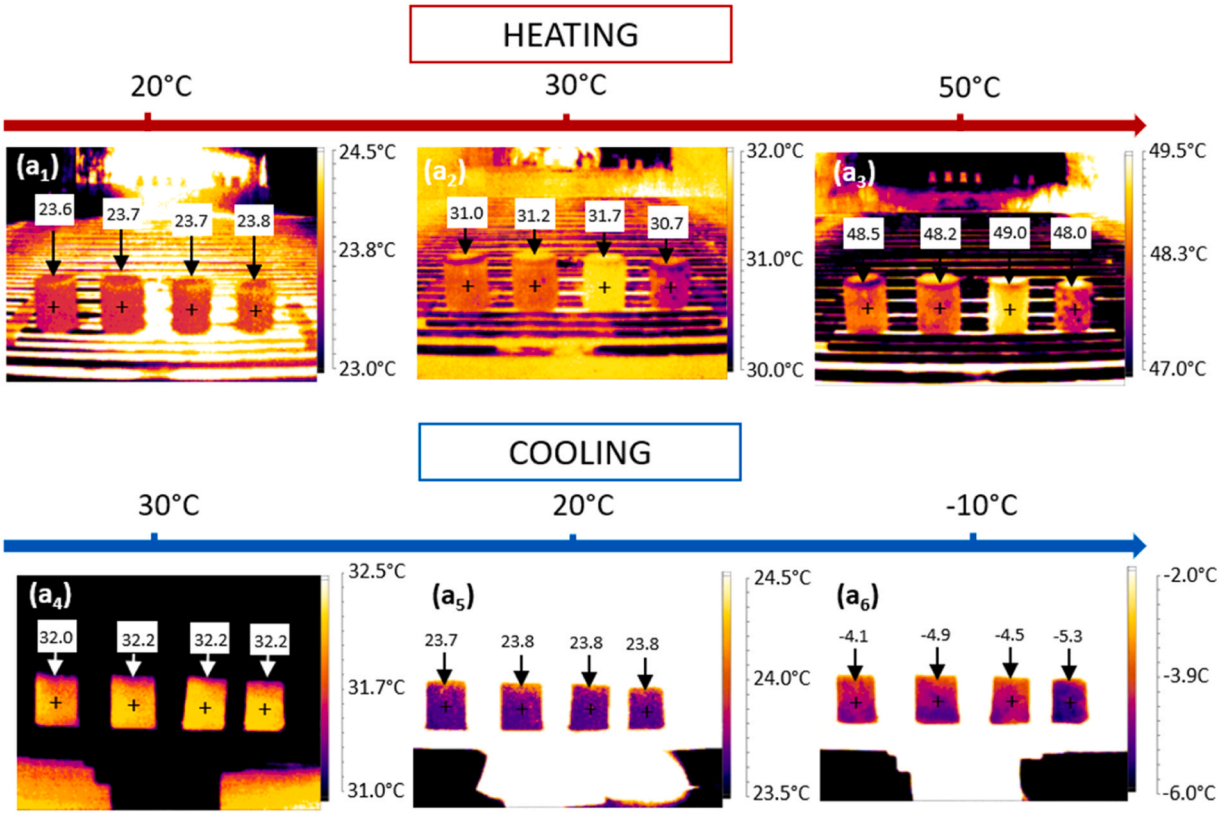

Fig. 10. Representative infrared thermographic maps of LM_P1820MK20 specimens during heating and cooling stages after durability exposure: (a_1-a_3) heating phase at 20, 30 and 50 °C, respectively; (a_4-a_6) cooling phase at 30, 20 and −10 °C, respectively.

reference.

At the highest heating setpoint (50 °C), a slight reduction in thermal agreement was observed for certain formulations under all durability scenarios (weathering, freeze-thaw, and salt attack). At this temperature, both PCM18 and PCM24 are fully in the liquid phase, and the thermal response is governed primarily by sensible heat transfer and matrix-related properties rather than latent heat effects. Under these conditions, durability-induced microstructural modifications or the presence of crystallised salts near the surface may cause minor variations in heat transfer, resulting in marginal reductions in thermal agreement without implying loss of PCM functionality.

The cooling stage (30, 20 and −10 °C) further confirmed the durability of MK-containing PCM mortars from a thermal perspective (Fig. 11). Consistent with the heating results, weathered specimens maintained high thermal agreement values across all formulations, demonstrating that realistic outdoor exposure has limited impact on functional thermal performance during cooling.

After freeze-thaw and salt exposure, a clear divergence emerged between mortars with and without metakaolin. MK-free formulations again exhibited thermal agreement values of 0%, reflecting the complete loss of functional equivalence with the intact reference. By comparison, MK-containing mortars retained high thermal agreement throughout the cooling stage, typically above 90% and, in several cases, approaching 100%, even under sub-zero conditions.

At −10 °C, a moderate decrease in thermal agreement was observed in some formulations (Fig. 11). At this stage, PCM crystallization and heat release are largely completed, and the thermal response becomes increasingly governed by sensible heat conduction and matrix continuity rather than latent heat effects. Under such conditions, microstructural alterations induced by severe ageing may slightly influence heat dissipation rates. Importantly, these deviations remain limited and do not indicate a loss of phase-change functionality but rather reflect the greater sensitivity of thermal agreement to matrix-related factors at the final cooling stage.

Overall, the thermal agreement analysis provides compelling evidence that metakaolin plays a decisive role in ensuring not only the structural durability of PCM-lime mortars but also the long-term preservation of their functional thermal behaviour. In line with the durability results discussed in Section 3.1, MK-containing mortars emerge as the most robust formulations, combining physical integrity with sustained thermal performance. While weathering exposure resulted in high thermal agreement across all mortars, only MK-containing formulations maintained thermal responses comparable to the intact reference after the most aggressive ageing mechanisms, namely freeze-thaw cycling and salt crystallization. This performance highlights the synergistic interaction between PCM incorporation and metakaolin addition, enabling lime-based renders to retain their thermal functionality even under extreme environmental conditions.

3.3.2. *Post-durability retention of heat storage and release capacity*

Differential Scanning Calorimetry (DSC) analyses were performed on specimens exposed to natural weathering, freeze-thaw cycling and salt crystallization in order to evaluate the post-durability retention of their latent heat storage and release capacity. The objective was to determine whether aggressive environmental exposure induced any loss of phase transition functionality in the microencapsulated PCMs embedded within the lime-based matrix. Melting (ΔH_m) and crystallization (ΔH_c) enthalpies were quantified and compared with those of the unaged references, as direct indicators of functional stability.

Following natural weathering, PCM-containing mortars preserved their latent heat storage and release capacity, with ΔH_m and ΔH_c values remaining practically unchanged relative to the unaged condition (Table 6 and Fig. 12). The variations observed were minor and fell within experimental uncertainty, indicating the absence of measurable functional degradation. The characteristic endothermic and exothermic peaks remained clearly defined and no significant shift in phase

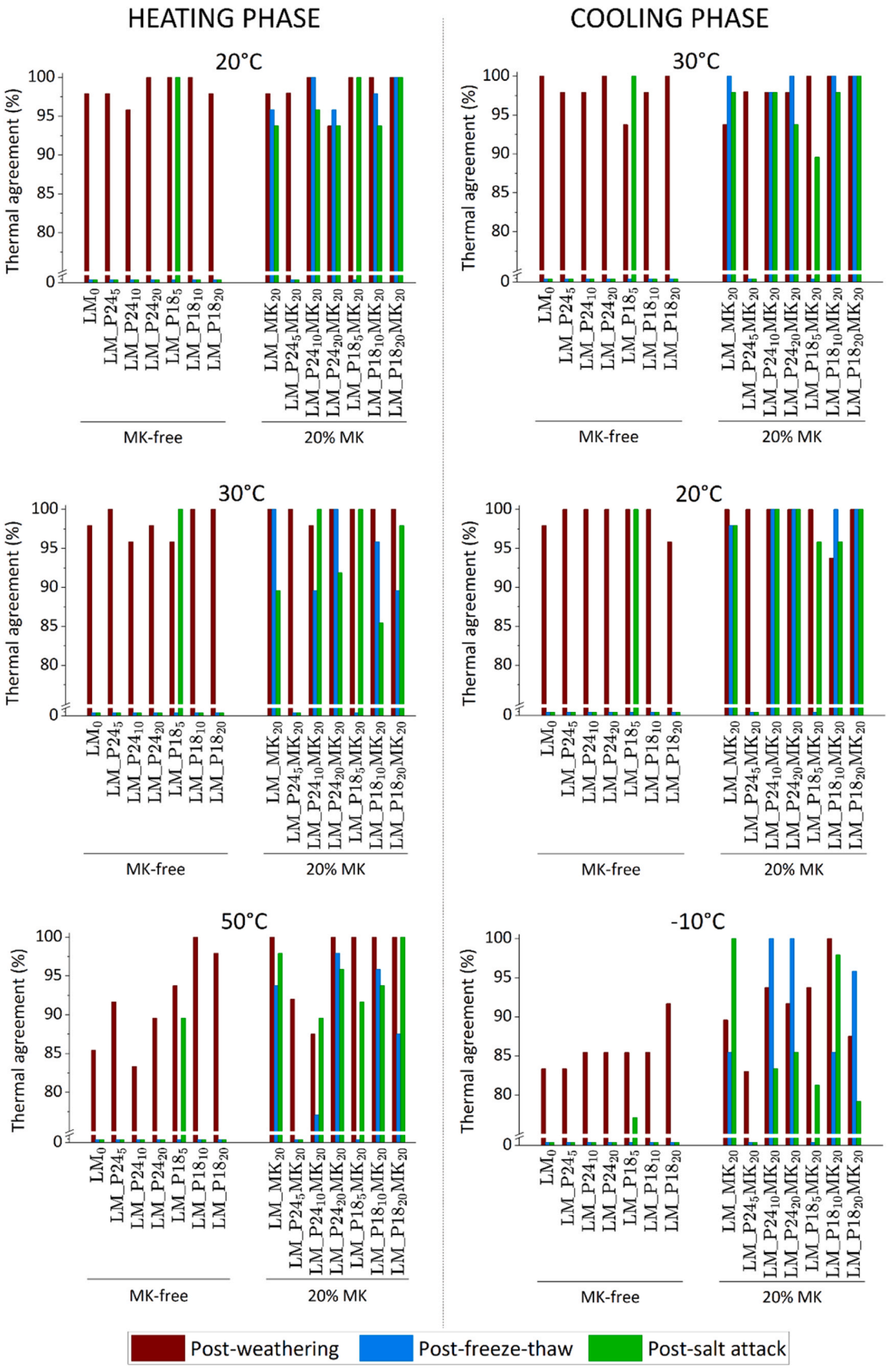

Fig. 11. Thermal agreement (%) of lime-based mortars after durability exposure (weathering, freeze-thaw and salt attack), evaluated at selected heating and cooling setpoints by comparison with the unaged specimen.

Table 6
Enthalpy values of melting (ΔH_m) and crystallization (ΔH_c) of PCM-lime mortars before and after ageing exposure.

		Mixture	Unaged	Post- weathering	Post- freeze-thaw	Post- salt attack
Latent energy storage (ΔH_m) (J/g)	MK-free	LM_P24$_5$	0.35 ± 0.01	0.46 ± 0.01	-	-
		LM_P24$_{10}$	0.67 ± 0.01	0.93 ± 0.01	-	-
		LM_P24$_{20}$	1.78 ± 0.01	1.81 ± 0.01	-	-
		LM_P18$_5$	0.55 ± 0.01	0.50 ± 0.01	-	0.54 ± 0.01
		LM_P18$_{10}$	0.69 ± 0.01	0.77 ± 0.01	-	-
		LM_P18$_{20}$	1.80 ± 0.01	2.41 ± 0.01	-	-
	20% MK	LM_P24$_5$MK$_{20}$	0.33 ± 0.01	0.49 ± 0.01	-	-
		LM_P24$_{10}$MK$_{20}$	0.61 ± 0.01	0.88 ± 0.01	1.05 ± 0.01	1.04 ± 0.09
		LM_P24$_{20}$MK$_{20}$	1.12 ± 0.01	1.10 ± 0.01	1.93 ± 0.01	2.75 ± 0.01
		LM_P18$_5$MK$_{20}$	0.44 ± 0.01	0.57 ± 0.01	-	0.42 ± 0.02
		LM_P18$_{10}$MK$_{20}$	0.86 ± 0.01	0.83 ± 0.01	0.95 ± 0.01	0.77 ± 0.01
		LM_P18$_{20}$MK$_{20}$	1.93 ± 0.01	2.08 ± 0.01	1.71 ± 0.01	1.88 ± 0.02
Latent energy release (ΔH_c) (J/g)	MK-free	LM_P24$_5$	0.41 ± 0.01	0.54 ± 0.01	-	-
		LM_P24$_{10}$	0.84 ± 0.01	1.10 ± 0.01	-	-
		LM_P24$_{20}$	2.00 ± 0.01	1.93 ± 0.01	-	-
		LM_P18$_5$	0.71 ± 0.01	0.60 ± 0.01	-	0.60 ± 0.01
		LM_P18$_{10}$	0.89 ± 0.01	0.94 ± 0.01	-	-
		LM_P18$_{20}$	2.13 ± 0.01	2.63 ± 0.01	-	-
	20% MK	LM_P24$_5$MK$_{20}$	0.38 ± 0.01	0.59 ± 0.01	-	-
		LM_P24$_{10}$MK$_{20}$	0.73 ± 0.01	1.01 ± 0.01	1.15 ± 0.01	1.29 ± 0.07
		LM_P24$_{20}$MK$_{20}$	1.38 ± 0.01	1.26 ± 0.01	2.16 ± 0.01	2.54 ± 0.01
		LM_P18$_5$MK$_{20}$	0.61 ± 0.01	0.70 ± 0.01	-	0.52 ± 0.04
		LM_P18$_{10}$MK$_{20}$	1.12 ± 0.01	1.10 ± 0.01	1.15 ± 0.01	0.92 ± 0.01
		LM_P18$_{20}$MK$_{20}$	1.93 ± 0.01	2.46 ± 0.01	1.94 ± 0.01	2.16 ± 0.03

Note: "-" indicates specimens that did not withstand the respective durability exposure.

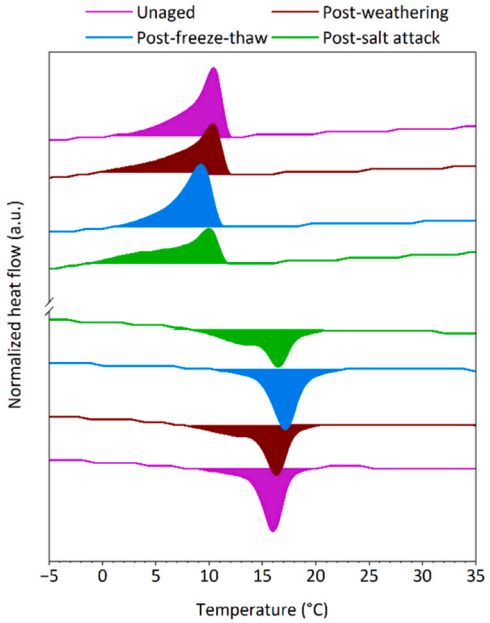

Fig. 12. DSC curves of LM_P18$_{10}$MK$_{20}$ mortar in the unaged state and after durability exposure (weathering, freeze-thaw, and salt attack), representative of the preserved latent heat performance of PCM-MK-lime mortars.

transition temperatures was detected (Fig. 12). These results confirm that natural environmental exposure did not alter the intrinsic phase transition behaviour of the microencapsulated PCMs embedded in the lime matrix.

After freeze-thaw cycles, representing an exceptionally demanding durability regime for porous lime-based materials, the DSC results confirmed that PCM-modified mortars preserved their latent heat storage and release capacity (Table 6 and Fig. 12). Both melting (ΔH_m) and crystallization (ΔH_c) enthalpies remained stable across all PCM-containing formulations, with only minor fluctuations. The characteristic endothermic and exothermic peaks remained clearly identifiable and well defined (Fig. 12), demonstrating that the microencapsulated PCMs maintained their thermal functionality despite repeated temperature fluctuations and moisture saturation.

After salt crystallization the thermal response remained equally robust. ΔH_m and ΔH_c values remained comparable to those of the unaged specimens, with only minor variations and no evidence of systematic enthalpy reduction (Table 6). The phase transition events remained clearly identifiable, demonstrating that the microencapsulated PCMs retained their ability to undergo reversible phase change after salt exposure (Fig. 12). These results indicate that salt-induced degradation mechanisms did not compromise the functional integrity of the PCM component within the lime-based matrix.

Overall, the close agreement between pre- and post-exposure DSC curves across all ageing protocols confirms that the latent heat storage and release capability of the mortars was fully preserved after natural weathering, freeze-thaw cycling and salt crystallization. The stability of enthalpy values and the absence of peak distortion demonstrate that the microencapsulated PCMs maintained their functional integrity, with no evidence of degradation. All the measured enthalpy values fall within, or in close proximity to, the range typically reported for comparable lime-based mortars incorporating microencapsulated PCMs (approximately 0.5–5 J/g) [21,22]. These results quantitatively support the excellent physical integrity observed after durability testing (Fig. 4 and Tables 3–4) and are fully consistent with the SEM observations, where microcapsules remained intact, well integrated within the matrix and free from visible damage (Fig. 7). Taken together, the findings highlight the compatibility between the lime-metakaolin binder and the microencapsulated PCMs, confirming that the binder behaves as a resilient matrix capable of preserving capsule integrity and ensuring sustained thermal performance even under highly demanding accelerated ageing conditions.

3.4. Cyclic thermal performance

3.4.1. Stability of latent heat storage and release capacity

Tables 7–8 summarise the statistical analysis of the melting and crystallization enthalpies of the PCM-enhanced formulations (Fig. 13). Key statistical descriptors, including mean, median, standard deviation (SD), absolute average deviation (AAD), range, maximum and minimum, were calculated to assess the thermal stability and cyclability PCM24 and PCM18 during repeated phase-change cycles. Together,

Table 7
Statistical analysis of DSC cyclability results during the melting process, including mean, median, standard deviation (SD), average absolute deviation (AAD), range and extreme values (maximum and minimum) for each PCM-enhanced mortar formulation.

Mixture	Mean (J/g)	Median (J/g)	Standard Deviation (SD) (J/g)	Average Absolute Deviation (AAD) (J/g)	Range (J/g)	Maximum Value (J/g)	Minimum Value (J/g)
LM_P24$_5$	0.84	0.84	0.01	0.01	0.04	0.86	0.82
LM_P24$_{10}$	0.97	0.96	0.05	0.04	0.18	1.08	0.90
LM_P24$_{20}$	3.36	3.36	0.04	0.04	0.14	3.42	3.28
LM_P18$_5$	0.85	0.85	0.01	0.01	0.03	0.87	0.84
LM_P18$_{10}$	1.18	1.18	0.01	0.01	0.03	1.20	1.17
LM_P18$_{20}$	3.19	3.19	0.05	0.04	0.14	3.26	3.12
LM_P24$_5$MK$_{20}$	0.75	0.75	0.01	0.01	0.02	0.76	0.74
LM_P24$_{10}$MK$_{20}$	1.31	1.31	0.02	0.02	0.06	1.34	1.28
LM_P24$_{20}$MK$_{20}$	3.43	3.44	0.04	0.04	0.13	3.50	3.37
LM_P18$_5$MK$_{20}$	0.81	0.81	0.01	0.01	0.02	0.82	0.80
LM_P18$_{10}$MK$_{20}$	1.28	1.28	0.01	0.01	0.02	1.29	1.26
LM_P18$_{20}$MK$_{20}$	1.98	1.98	0.01	0.01	0.04	1.99	1.96

Table 8
Statistical analysis of DSC cyclability results during the crystallization process, including mean, median, standard deviation (SD), average absolute deviation (AAD), range and extreme values (maximum and minimum) for each PCM-enhanced mortar formulation.

Mixture	Mean (J/g)	Median (J/g)	Standard Deviation (SD) (J/g)	Average Absolute Deviation (AAD) (J/g)	Range (J/g)	Maximum Value (J/g)	Minimum Value (J/g)
LM_P24$_5$	0.80	0.80	0.04	0.03	0.21	0.94	0.73
LM_P24$_{10}$	0.81	0.88	0.04	0.04	0.13	0.97	0.83
LM_P24$_{20}$	3.12	3.11	0.03	0.03	0.12	3.19	3.07
LM_P18$_5$	0.67	0.66	0.01	0.01	0.07	0.70	0.64
LM_P18$_{10}$	0.85	0.84	0.02	0.02	0.09	0.90	0.81
LM_P18$_{20}$	2.68	2.68	0.05	0.04	0.17	2.78	2.61
LM_P24$_5$MK$_{20}$	0.76	0.76	0.01	0.01	0.04	0.77	0.73
LM_P24$_{10}$MK$_{20}$	1.22	1.22	0.01	0.01	0.05	1.24	1.19
LM_P24$_{20}$MK$_{20}$	3.12	3.12	0.03	0.03	0.10	3.18	3.08
LM_P18$_5$MK$_{20}$	0.56	0.56	0.02	0.01	0.08	0.61	0.53
LM_P18$_{10}$MK$_{20}$	0.94	0.94	0.01	0.01	0.06	0.97	0.91
LM_P18$_{20}$MK$_{20}$	1.63	1.63	0.02	0.02	0.09	1.68	1.59

these indicators provide a quantitative evaluation of the reproducibility and reliability of the latent heat response under cyclic thermal loading.

The melting enthalpy results (Table 7) confirm the high thermal stability of all formulations. For instance, LM_P24$_5$ exhibited a mean absorbed heat of 0.840 J/g (median = 0.839 J/g), with a very low dispersion (SD = 0.009 J/g, AAD = 0.007 J/g, range = 0.037 J/g), indicating minimal variability between cycles. Increasing the PCM content, as in LM_P24$_{20}$, led to a proportional increase in energy storage capacity (mean = 3.355 J/g), while maintaining limited variability (median = 3.361 J/g, SD = 0.042 J/g, AAD = 0.036 J/g, range = 0.139 J/g). These results demonstrate that higher PCM loading enhances latent heat storage without compromising thermal repeatability.

A similar trend was observed for PCM18-based mortars. LM_P18$_{10}$ showed a mean absorbed heat of 1.184 J/g (median = 1.183 J/g), with very low variability (SD = 0.010 J/g, AAD = 0.010 J/g, range = 0.033 J/g), confirming stable behaviour across repeated cycles. The formulation with the highest PCM18 content, LM_P18$_{20}$, reached a mean value of 3.187 J/g (median = 3.188 J/g, AAD = 0.039 J/g), further demonstrating the robustness of the system even at elevated PCM concentrations.

Across all formulations, the consistently low SD and AAD values highlight the uniformity of latent heat exchange during repeated heating and cooling. The reproducibility in both melting and crystallization enthalpies confirms that the microencapsulated PCMs preserved their phase-change integrity throughout cyclic testing. This high degree of thermal stability is essential for long-term performance, supporting the reliable integration of PCM-lime mortars in sustainable and energy-efficient building envelopes.

These quantitative results are further corroborated by Fig. 13, which shows the overlapping DSC curves recorded over 40 thermal cycles. The near-complete superposition of the melting and crystallization peaks evidences the high thermal stability and repeatability of the PCMs, with no observable degradation, peak shift, or alteration in thermal response throughout cycling.

The crystallization results (Table 8) further confirms the robustness of the PCMs' thermal performance. For LM_P24$_{10}$MK$_{20}$, the mean released heat is 1.216 J/g (median = 1.217 J/g), with very limited variability (SD = 0.011 J/g, AAD = 0.009 J/g, range = 0.051 J/g), indicating stable and reproducible heat release during cycling. Similarly, LM_P24$_{20}$MK$_{20}$ exhibits a mean crystallization enthalpy of 3.122 J/g (median = 3.120 J/g, AAD = 0.025 J/g), demonstrating consistent and uniform latent heat release even after extensive thermal cycling.

PCM18-based mortars display comparable behaviour. LM_P18$_{10}$MK$_{20}$ shows a mean released heat of 0.942 J/g (median = 0.941 J/g, AAD = 0.009 J/g, range = 0.063 J/g), confirming its high thermal stability. The higher PCM-content formulation, LM_P18$_{20}$, achieves a mean value of 2.679 J/g (median = 2.675 J/g, AAD = 0.036 J/g), further supporting the sustained and repeatable performance of the system across successive crystallization cycles.

The direct comparison between PCM24 and PCM18 highlights their excellent cyclability across all tested formulations. Both materials exhibit consistently low SD and AAD values, while the close correspondence between mean and median enthalpy values confirms highly stable and repeatable phase-change behaviour. These results underscore their suitability for long-term thermal energy storage applications. Fig. 13 visually corroborates this stability, as the overlapping phase-change curves remain virtually unchanged over 40 cycles, reinforcing the exceptional thermal reliability of both PCMs.

The minimal variability observed in key statistical descriptors, even after numerous heating and cooling cycles, demonstrates that the PCMs repeatedly absorb and release heat with negligible fluctuations. Such

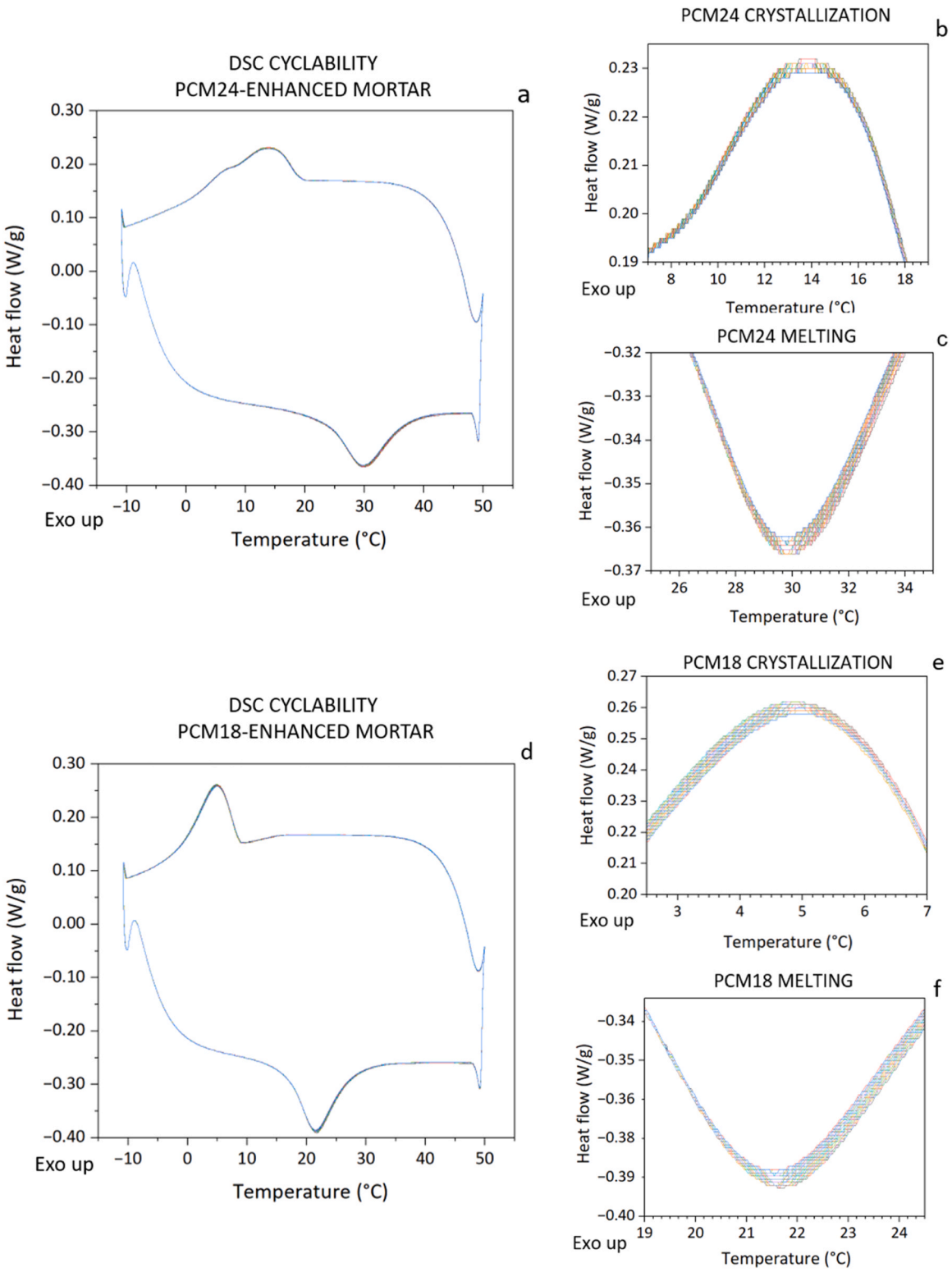

Fig. 13. DSC thermal cycling analysis over 40 successive cycles for lime mortars incorporating PCMs. (a) Complete phase change cycles of LM_P24$_{20}$MK$_{20}$; (b) crystallization detail; (c) melting detail; (d) complete phase change cycles of LM_P18$_{20}$; (e) crystallization detail; (f) melting detail. The overlapping curves demonstrate the excellent stability and reproducibility of the PCMs' thermal behaviour across repeated phase transitions.

reproducibility is fundamental for ensuring dependable long-term thermal performance in building materials, where sustained efficiency and operational stability throughout the service life are essential.

Moreover, the demonstrated thermal stability of the PCMs contributes directly to the overall sustainability of PCM-lime mortars by enhancing energy efficiency and reducing thermal fluctuations within building envelopes. Their capacity to undergo repeated phase transitions without degradation confirms their potential as a robust passive energy-management strategy, supporting durable, low-maintenance, and environmentally responsible construction solutions.

3.4.2. Long-term energy efficiency enhancement

Previous studies have demonstrated that the incorporation of PCMs into lime-based renders can significantly improve energy efficiency [21]. In the present study, however, the focus was placed on evaluating the cyclic stability of this improvement, that is, whether the enhanced thermal performance of the mortars could be maintained under repeated heating-cooling cycles. To address this objective, a representative subset of formulations was selected, ensuring that the findings would be indicative of the overall behaviour of the PCM-modified systems.

The results of the cyclic hotbox tests are summarized in Tables 9–10, which present the evolution of temperature variations recorded over 40 consecutive thermal cycles. These data quantify the thermal buffering capacity of the PCM-bearing renders, expressed both as the attenuation of maximum and minimum temperature peaks relative to the reference mortars (Table 9) and as the temperature differentials observed throughout each complete cycle (Table 10). By analysing these parameters over the entire testing programme, it was possible to evaluate not only the initial thermal benefits associated with PCM incorporation but also the persistence, stability, and reproducibility of these benefits under prolonged cyclic thermal loading.

At the heating peaks (Table 9), mortars incorporating higher PCM contents (20%) exhibited the most pronounced attenuation of maximum temperatures. LM_P24$_5$MK$_{20}$ and LM_P18$_{20}$MK$_{20}$ achieved average damping values of 1.40 °C and 1.00 °C, respectively. As expected, formulations with lower PCM content (5%) displayed smaller, yet still significant, buffering effects, with average reductions of 0.79 °C for LM_P24$_5$ and 0.87 °C for LM_P18$_5$. Across all mixtures, the statistical descriptors indicate stable behaviour throughout the 40 cycles, confirming the reproducible and cyclable nature of the thermal response, irrespective of PCM dosage.

A similar trend was observed at the cooling peaks (Table 9), where mortars containing 20% PCM again showed the most substantial temperature attenuation, averaging 0.77 °C for LM_P18$_{20}$MK$_{20}$ and 0.64 °C for LM_P24$_5$MK$_{20}$. Formulations with 5% PCM exhibited more moderate reductions, close to 0.1°C, but maintained consistent statistical stability over the full testing period. These results demonstrate that both low- and high-dosage PCM mortars preserve their thermal buffering efficiency under prolonged cyclic exposure, with higher PCM contents amplifying the magnitude of the effect.

The temperature variations recorded throughout the entire heating phase are presented in Table 10. The data confirm that PCM incorporation leads to substantial attenuation of temperature rise during each cycle, with the buffering effect increasing proportionally with PCM content. Mortars containing 20% PCM exhibited the highest average temperature differentials, reaching 3.01 °C for LM_P24$_5$MK$_{20}$ and 2.58 °C for LM_P18$_{20}$MK$_{20}$. Formulations with 5% PCM showed slightly lower, yet still significant, reductions of 1.82 °C for LM_P24$_5$ and 2.23 °C for LM_P18$_5$. In all cases, standard deviations remained below 0.15 °C, and the close agreement between mean and median values confirms the high reproducibility of the results across 40 cycles. Overall, these findings demonstrate that PCM-bearing renders effectively moderate temperature evolution during the heating phase and maintain this performance consistently under extended cyclic thermal loading.

During the cooling phase (Table 10), a comparable trend was observed. Mortars containing 20% PCM again exhibited the most pronounced buffering effect, with mean temperature differentials of 1.51 °C for LM_P24$_5$MK$_{20}$ and 1.41 °C for LM_P18$_{20}$MK$_{20}$, compared with 0.37 °C and 0.36 °C for LM_P24$_5$ and LM_P18$_5$, respectively. Although the absolute magnitudes were lower than those recorded during the heating phase, the effect remained consistent throughout all 40 cycles, as reflected by the narrow data ranges and low standard deviations. This sustained behaviour confirms the ability of PCM-bearing mortars to effectively moderate temperature fluctuations during both heating and cooling, demonstrating stable and repeatable energy-storage performance.

To further quantify the cumulative thermal buffering capacity, the integrals of relative energy exchange (Q*) were calculated from the temperature difference curves ($\Delta T = T_{reference\ hotbox} - T_{PCM\ hotbox}$) over time. This parameter provides a global measure of the total thermal modulation achieved by each mortar across the 40 thermal cycles. The statistical analysis of Q* is summarized in Table 11.

The mean values confirm that mortars with higher PCM contents exhibit greater energy exchange capacity, consistent with the stronger temperature damping trends identified in Tables 9–10. The highest Q* values were recorded for LM_P24$_5$MK$_{20}$ and LM_P18$_{20}$MK$_{20}$, reaching approximately 2.5×10^5 °C·s/m^2 and 1.9×10^5 °C·s/m^2, respectively. Formulations containing 5% PCM showed proportionally lower, but still substantial integrals, 1.3 × 105 °C·s/m2 for LM_P24$_5$ and 1.4×10^5 °C·s/m^2 for LM_P18$_5$. Standard deviations remained within the same order of magnitude across all formulations, and the narrow data ranges further confirm the reproducibility and stability of the thermal response under prolonged cyclic exposure.

These results reinforce the trends observed in the temperature-buffering analyses, confirming that the cumulative thermal performance of PCM-bearing mortars remains stable under prolonged cyclic exposure. The consistent Q* values across all cycles demonstrate that the materials retain their capacity for effective heat exchange, underscoring the long-term reliability of their energy-saving functionality. This stability is further illustrated in Fig. 14, which presents the temperature-time curves for the LM_P24$_{20}$MK$_{20}$ formulation. The near-complete overlap of the successive cycles indicates that the material's thermal response remains both stable and highly repeatable throughout the entire testing programme.

4. Conclusions

This study presents a comprehensive evaluation of the long-term viability of lime-based renders incorporating microencapsulated phase

Table 9
Statistical analysis of temperature buffering at heating peaks (maximum temperatures) and cooling peaks (minimum temperatures) over 40 hotbox cycles.

	Heating buffering (ΔT at maximum peaks) (°C)						
Mixture	Mean	Median	Standard Deviation (SD)	Average Absolute Deviation (AAD)	Range	Maximum Value	Minimum Value
LM_P24$_5$	0.79	0.81	0.09	0.07	0.34	0.94	0.60
LM_P18$_5$	0.87	0.87	0.05	0.04	0.19	0.95	0.77
LM_P24$_{20}$MK$_{20}$	1.40	1.46	0.13	0.11	0.51	1.56	1.05
LM_P18$_{20}$MK$_{20}$	1.00	1.00	0.10	0.08	0.38	1.14	0.76
	Cooling buffering (|ΔT| at minimum peaks) (°C)						
Mixture	Mean	Median	Standard Deviation (SD)	Average Absolute Deviation (AAD)	Range	Maximum Value	Minimum Value
LM_P24$_5$	0.09	0.09	0.02	0.02	0.09	0.15	0.06
LM_P18$_5$	0.08	0.07	0.03	0.02	0.13	0.13	0.00
LM_P24$_{20}$MK$_{20}$	0.64	0.64	0.03	0.02	0.16	0.76	0.60
LM_P18$_{20}$MK$_{20}$	0.77	0.76	0.03	0.03	0.13	0.85	0.72

During the cooling phase, ΔT = Treference hotbox - TPCM hotbox is negative because the reference (PCM free) hotbox reaches lower temperatures than the PCM-bearing one. Accordingly, absolute values (|ΔT|) are reported to represent the magnitude of the thermal buffering effect.

Table 10
Statistical analysis of temperature buffering during the heating phase (ΔT across the full heating phase over 40 hotbox cycles) and cooling phase (ΔT across the full cooling phase over 40 hotbox cycles).

	Heating buffering (ΔT at heating phase) (°C)						
Mixture	Mean	Median	Standard Deviation (SD)	Average Absolute Deviation (AAD)	Range	Maximum Value	Minimum Value
LM_P24$_5$	1.82	1.83	0.06	0.05	0.23	1.93	1.70
LM_P18$_5$	2.23	2.23	0.06	0.04	0.28	2.35	2.08
LM_P24$_{20}$MK$_{20}$	3.01	2.99	0.14	0.12	0.61	3.30	2.69
LM_P18$_{20}$MK$_{20}$	2.58	2.57	0.12	0.09	0.59	2.94	2.34
	Cooling buffering (*|ΔT| at cooling phase) (°C)						
Mixture	Mean	Median	Standard Deviation (SD)	Average Absolute Deviation (AAD)	Range	Maximum Value	Minimum Value
LM_P24$_5$	0.37	0.36	0.05	0.04	0.19	0.30	0.49
LM_P18$_5$	0.36	0.37	0.05	0.04	0.18	0.25	0.44
LM_P24$_{20}$MK$_{20}$	1.51	1.51	0.05	0.04	0.27	1.41	1.68
LM_P18$_{20}$MK$_{20}$	1.41	1.40	0.02	0.02	0.07	1.38	1.45

* During the cooling phase, $\Delta T = T_{reference\ hotbox} - T_{PCM\ hotbox}$ is negative because the reference (PCM free) hotbox reaches lower temperatures than the PCM-bearing one. Accordingly, absolute values ($|\Delta T|$) are reported to represent the magnitude of the thermal buffering effect.

Table 11
Statistical analysis of relative energy exchanged (Q*) during cyclic hotbox testing over 40 cycles.

	Relative energy exchanged (°C·s /m^2)						
Mixture	Mean	Median	Standard Deviation (SD)	Average Absolute Deviation (AAD)	Range	Maximum Value	Minimum Value
LM_P24$_5$	$1.3 \cdot 10^5$	$1.3 \cdot 10^5$	$4.7 \cdot 10^3$	$3.6 \cdot 10^3$	$2.1 \cdot 10^4$	$1.4 \cdot 10^5$	$1.2 \cdot 10^5$
LM_P18$_5$	$1.4 \cdot 10^5$	$1.4 \cdot 10^5$	$5.1 \cdot 10^3$	$3.9 \cdot 10^3$	$2.3 \cdot 10^4$	$1.5 \cdot 10^5$	$1.2 \cdot 10^5$
LM_P24$_{20}$MK$_{20}$	$2.5 \cdot 10^5$	$2.5 \cdot 10^5$	$4.6 \cdot 10^3$	$3.6 \cdot 10^3$	$2.2 \cdot 10^4$	$2.6 \cdot 10^5$	$2.4 \cdot 10^5$
LM_P18$_{20}$MK$_{20}$	$1.9 \cdot 10^5$	$1.9 \cdot 10^5$	$4.4 \cdot 10^3$	$3.5 \cdot 10^3$	$1.9 \cdot 10^4$	$2.0 \cdot 10^5$	$1.8 \cdot 10^5$

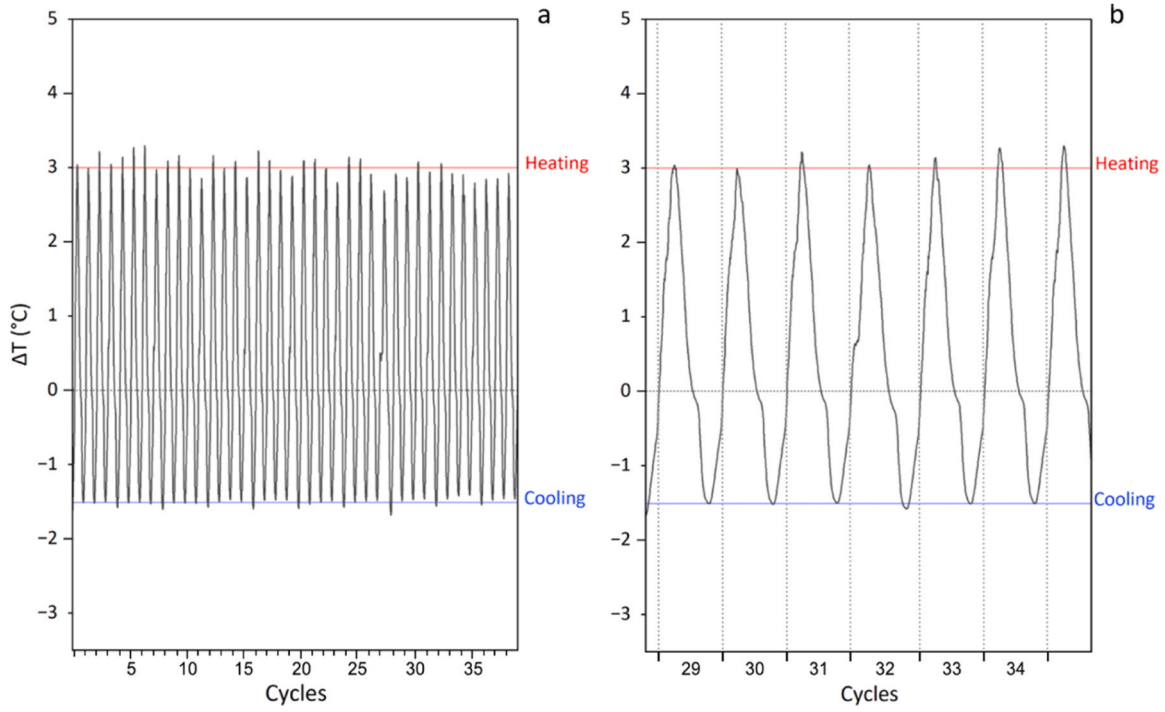

Fig. 14. Temperature-time profiles of the temperature difference (ΔT = TLM_MK$_{20}$ - T LM_P24$_{20}$MK$_{20}$) recorded over 40 heating-cooling cycles for LM_P2420MK20: (a) complete sequence of 40 cycles showing highly consistent ΔT amplitudes, evidencing the repeatable and cyclable nature of the thermal response; (b) detail of six consecutive cycles illustrating the stability and reproducibility of temperature evolution during both heating and cooling phases.

change materials (PCMs), explicitly integrating durability performance, microstructural and mechanical evolution, and preservation of functional thermal behaviour. Rather than limiting durability to macroscopic damage indicators, the findings demonstrate that a meaningful evaluation of sustainability must also verify the retention of thermal performance and energy-related functionality after exposure to severe environmental conditions. The key findings of this study are summarised below:

- Durability performance is strongly governed by mortar formulation. While all systems remained stable under natural weathering, PCM-bearing mortars without metakaolin failed prematurely under freeze-thaw and salt crystallization, whereas PCM-metakaolin formulations successfully completed the full set of durability cycles.

- Optimized PCM-metakaolin mortars exhibited enhanced resistance to aggressive ageing conditions, reaching low damage levels after freeze-thaw cycling (damage score 1–2) and maintaining structural stability under salt attack (damage score ~6).
- Post-durability microstructural analyses revealed preservation of a coherent and refined pore network, with no evidence of pore coarsening. SEM observations confirmed that the microencapsulated PCMs remained intact and well-integrated within the matrix after all ageing regimes.
- Mechanical performance was maintained or improved after durability exposure. PCM-metakaolin mortars showed increases in compressive strength of up to 460% following salt exposure, confirming the robustness and resilience of the optimized lime matrix.
- Functional thermal behaviour was preserved after severe ageing. Thermal agreement values generally exceeded 90% and reached 100% in several cases, indicating that optimized formulations retained a thermal response comparable to that of the intact mortar, whereas non-optimized systems lost functional equivalence due to structural failure.
- Latent heat storage and release capacity remained stable after durability exposure. Stable melting and crystallization enthalpy values support the retention of phase-transition behaviour.
- Extended cyclic testing confirmed highly reproducible thermal behaviour over repeated heating-cooling cycles, demonstrating that the microencapsulated PCMs maintained their phase-change functionality without degradation or thermal fatigue. Consistent results at both material and laboratory envelope scales further confirm that the energy-buffering effect remains stable and cyclable over time.

Overall, the findings demonstrate that PCM-enhanced lime renders can only be considered truly sustainable when durability, mechanical resilience, and long-term thermal functionality are addressed simultaneously. When optimally formulated with metakaolin, these materials combine resistance to aggressive environmental exposure with persistent and repeatable thermal performance. This integrated robustness supports their technical feasibility as durable, energy-efficient solutions for long-term retrofit applications in the built environment.

CRediT authorship contribution statement

Andrea Rubio-Aguinaga: Writing – original draft, Visualization, Validation, Methodology, Investigation, Formal analysis, Data curation, Conceptualization. **José María Fernández:** Writing – review & editing, Conceptualization. **Loucas Kyriakou:** Writing – review & editing, Data curation, Conceptualization. **Alvarez José Ignacio:** Writing – review & editing, Visualization, Supervision, Resources, Project administration, Funding acquisition, Conceptualization. **Íñigo Navarro-Blasco:** Supervision, Resources, Project administration, Methodology, Funding acquisition, Conceptualization.

Declaration of Competing Interest

The authors declare that they have no known competing financial interests or personal relationships that could have appeared to influence the work reported in this paper.

Acknowledgements

The authors sincerely thank Cristina Luzuriaga for her technical support. We also acknowledge the material contributions from Calinsa S. A. Navarra and CTH Navarra.

This work was co-funded by the European Union's Horizon Europe research and innovation programme, under Grant Agreement No 101123293 (SINCERE- The Second Life of Modern Period Architecture: Resilient and Adaptive Renovation towards Net-Zero Carbon Heritage Buildings) and by Gobierno de España, Ministerio de Ciencia e Innovación MICINN/AEI/10.13039/501100011033, grant PID2020–119975RB-I00, LIMORTHER. Andrea Rubio-Aguinaga has been granted a fellowship of the programme of the Gobierno de España, Ministerio de Universidades FPU21/04961.

Data Availability

Data will be made available on request.

References

[1] United Nations Environment Programme, Global Status Report for Buildings and Construction 2022: Towards a Zero-emission, Efficient and Resilient Buildings and Construction Sector, Nairobi, 2022, 2022.
[2] European Commission, A Renovation Wave for Europe – Greening our buildings, creating jobs, improving lives, Brussels, 2020.
[3] European Commission, The European Green Deal, Brussels, 2019.
[4] European Commission, Nearly-zero energy and zero-emission buildings. Energy Performance of Buildings Directive (EPBD) recast – directive (EU) 2024/1275, 2025.
[5] M.D. Alba-Rodríguez, A. Martínez-Rocamora, P. González-Vallejo, A. Ferreira-Sánchez, M. Marrero, Building rehabilitation versus demolition and new construction: Economic and environmental assessment, Environ. Impact Assess. Rev. 66 (2017) 115–126, https://doi.org/10.1016/j.eiar.2017.06.002.
[6] B. Wu, R. Maalek, Renovation or Redevelopment: The Case of Smart Decision-Support in Aging Buildings, Smart Cities 6 (2023) 1922–1936, https://doi.org/10.3390/smartcities6040089.
[7] F. Pittau, D. Giacomel, G. Iannaccone, L. Malighetti, Environmental consequences of refurbishment versus demolition and reconstruction: a comparative life cycle assessment of an italian case study, J. Green. Build. 15 (2020) 155–172.
[8] A. Säynäjoki, J. Heinonen, S. Junnila, A scenario analysis of the life cycle greenhouse gas emissions of a new residential area, Environ. Res. Lett. 7 (2012), https://doi.org/10.1088/1748-9326/7/3/034037.
[9] F. Pomponi, A. Moncaster, Embodied carbon mitigation and reduction in the built environment What does the evidence say? J. Environ. Manag. 181 (2016) 687–700, https://doi.org/10.1016/j.jenvman.2016.08.036.
[10] W.M. Fei, A. Opoku, K. Agyekum, J.A. Oppon, V. Ahmed, C. Chen, K.L. Lok, The Critical Role of the Construction Industry in Achieving the Sustainable Development Goals (SDGs): Delivering Projects for the Common Good, Sustainability 13 (2021), https://doi.org/10.3390/su13169112.
[11] C. Rodriguez-Navarro, T. Ilic, E. Ruiz-Agudo, K. Elert, Carbonation mechanisms and kinetics of lime-based binders: An overview, Cem. Concr. Res. 173 (2023), https://doi.org/10.1016/j.cemconres.2023.107301.
[12] L.F. Bing, M.J. Ma, L.L. Liu, J.Y. Wang, L. Niu, F.M. Xi, An investigation of the global uptake of CO2 by lime from 1930 to 2020, Earth Syst. Sci. Data 15 (2023) 2431–2444, https://doi.org/10.5194/essd-15-2431-2023.
[13] F.Pietro Campo, M. Grosso, Lime Based Construction Materials as a Carbon Sink, Key Eng. Mater. 922 (2022) 139–145, https://doi.org/10.4028/p-t8k30r.
[14] A. Manoharan, C. Umarani, Lime Mortar, a Boon to the Environment: Characterization Case Study and Overview, Sustainability 14 (2022), https://doi.org/10.3390/su14116481.
[15] M. Do Rosário Veiga, A. Fragata, A.L. Velosa, A.C. Magalhães, G. Margalha, Lime-based mortars: Viability for use as substitution renders in historical buildings, Int. J. Archit. Herit. 4 (2010) 177–195, https://doi.org/10.1080/15583050902914678.
[16] J. Ryan, M. Bussmann, N. DeMartini, CFD Modelling of Calcination in a Rotary Lime Kiln, PROCESSES 10 (2022), https://doi.org/10.3390/pr10081516.
[17] A. Rubio-Aguinaga, L. Kyriakou, J.M. Fernández, I. Navarro-Blasco, S. Pavia, J. I. Álvarez, Sustainability of PCM-lime mortars for heritage retrofitting: Carbon footprint and impact on energy demand across climates, Case Stud. Constr. Mater. 23 (2025) e05294, https://doi.org/10.1016/j.cscm.2025.e05294.
[18] J.T. Ju, H.B. Cao, W.K. Guo, N. Luo, Q.M. Zhang, Y.G. Wang, Experimental Study on Calcination of Portland Cement Clinker Using Different Contents of Stainless Steel Slag, Materials 17 (2024), https://doi.org/10.3390/ma17102305.
[19] F. Masdeu, C. Carmona, G. Horrach, J. Muñoz, Effect of iron (III) oxide powder on thermal conductivity and diffusivity of lime mortar, Materials 14 (2021) 1–14, https://doi.org/10.3390/ma14040998.
[20] A. Sarcinella, J.L.B. De Aguiar, M. Lettieri, S. Cunha, M. Frigione, Thermal Performance of Mortars Based on Different Binders and Containing a Novel Sustainable Phase Change Material (PCM), MATERIALS 13 (2020), https://doi.org/10.3390/ma13092055.
[21] A. Rubio-Aguinaga, J.M. Fernández, Í. Navarro-Blasco, J.I. Álvarez, Air lime renders with microencapsulated phase change materials: Assessment of microstructural and thermal properties, Constr. Build. Mater. 452 (2024) 138862, https://doi.org/10.1016/j.conbuildmat.2024.138862.

[22] A. Rubio-Aguinaga, L. Kyriakou, J.M. Fernández, Í. Navarro-Blasco, J.I. Álvarez, Microstructural analysis of bio-based PCM-enhanced lime mortars: Durability and energy efficiency for sustainable buildings, Constr. Build. Mater. 481 (2025) 141569, https://doi.org/10.1016/j.conbuildmat.2025.141569.
[23] M. Theodoridou, L. Kyriakou, I. Ioannou, PCM-enhanced Lime Plasters for Vernacular and Contemporary Architecture, Energy Procedia 97 (2016) 539–545, https://doi.org/10.1016/j.egypro.2016.10.070.
[24] A. Sarcinella, Physical Properties of an Eco-Sustainable, Form-Stable Phase Change Material Included in Aerial-Lime-Based Mortar Intended for Different Climates, MATERIALS 15 (2022) 1192.
[25] M. Frigione, M. Lettieri, A. Sarcinella, J.B. de Aguiar, Sustainable polymer-based Phase Change Materials for energy efficiency in buildings and their application in aerial lime mortars, Constr. Build. Mater. 231 (2020) 117149, https://doi.org/10.1016/j.conbuildmat.2019.117149.
[26] V.V. Rao, R. Parameshwaran, V.V. Ram, PCM-mortar based construction materials for energy efficient buildings: A review on research trends, Energy Build. 158 (2018) 95–122, https://doi.org/10.1016/j.enbuild.2017.09.098.
[27] K.Y. Weng, X.Y. Xu, Y.Y. Chen, X.L. Li, C.Y. Qing, D.Q. Zou, Development and applications of multifunctional microencapsulated PCMs: A comprehensive review, Nano Energy 122 (2024), https://doi.org/10.1016/j.nanoen.2024.109308.
[28] L.F. Cabeza, A. Castell, G. Pérez, Life cycle assessment (LCA) of phase change materials (PCMs) used in buildings, in: F. PachecoTorgal, L.F. Cabeza, J. Labrincha, A. DeMagalhaes (Eds.), Eco-Efficient Construction and Building Materials: Life Cycle Assessment (LCA), Eco-Labelling and Case Studies, 2014, pp. 287–310, https://doi.org/10.1533/9780857097729.2.287.
[29] S.S. Lucas, J.L. Barroso de Aguiar, Evaluation of latent heat storage in mortars containing microencapsulated paraffin waxes – a selection of optimal composition and binders, Heat. Mass Transf. /Waerme- Und Stoff. (2019), https://doi.org/10.1007/s00231-019-02594-1.
[30] F. Ascione, N. Bianco, R.F. De Masi, G.M. Mauro, G.P. Vanoli, Design of the Building Envelope: A Novel Multi-Objective Approach for the Optimization of Energy Performance and Thermal Comfort, Sustainability 7 (2015) 10809–10836, https://doi.org/10.3390/su70810809.
[31] J.E. Huang, S.S. Wang, F.H. Teng, W. Feng, Thermal performance optimization of envelope in the energy-saving renovation of existing residential buildings, Energy Build. 247 (2021), https://doi.org/10.1016/j.enbuild.2021.111103.
[32] D. Kumar, M. Alam, J.G. Sanjayan, Retrofitting Building Envelope Using Phase Change Materials and Aerogel Render for Adaptation to Extreme Heatwave: A Multi-Objective Analysis Considering Heat Stress, Energy, Environment, and Cost, Sustainability 13 (2021), https://doi.org/10.3390/su131910716.
[33] C. Ornelas, J.M. Guedes, I. Breda-vázquez, Cultural built heritage and intervention criteria: A systematic analysis of building codes and legislation of Southern European countries, J. Cult. Herit. 20 (2016) 725–732, https://doi.org/10.1016/j.culher.2016.02.013.
[34] A. Rubio-Aguinaga, J.M. Fernandez, I. Navarro-Blasco, J.I. Alvarez, Study on the Interaction of Polymeric Chemical Additives with Phase Change Materials in Air Lime Renders, Polym. (Basel) 16 (2024) 1121, https://doi.org/10.3390/polym16081121.
[35] J. Feijoo, M.A. Alvarez-Feijoo, R. Fort, E. Arce, D. Ergenç, Effects of paraffin additives, as phase change materials, on the behavior of a traditional lime mortar, Constr. Build. Mater. 361 (2022) 129734, https://doi.org/10.1016/j.conbuildmat.2022.129734.
[36] M. Frigione, M. Lettieri, A. Sarcinella, Phase Change Materials for Energy Efficiency in Buildings and Their Use in Mortars, Materials 12 (2019) 1260, https://doi.org/10.3390/ma12081260.
[37] B.P. Jelle, S.E. Kalnaes, Phase Change Materials for Application in Energy-Efficient Buildings. in: Cost-Effective Energy Efficient Building Retrofitting, Woodhead Publishing, 2017, https://doi.org/10.1016/B978-0-08-101128-7.00003-4.
[38] C.V. Podara, I.A. Kartsonakis, C.A. Charitidis, Towards phase change materials for thermal energy storage: classification, improvements and applications in the building sector, Appl. Sci. 11 (2021) 1490.
[39] S. Cunha, J. Aguiar, V. Ferreira, Durability of mortars with incorporation of phase change materials microcapsules, Rom. J. Mater. 47 (2017) 166–175.
[40] F. PachecoTorgal, L.F. Cabeza, J. Labrincha, A. DeMagalhaes, eds., Eco-Efficient Construction and Building Materials: Life Cycle Assessment (LCA), Eco-Labelling and Case Studies, in: Eco-Efficient Construction and Building Materials: Life Cycle Assessment (LCA), Eco-Labelling and Case Studies, 2014: pp. 1-617.
[41] A. Wadee, P. Walker, N. Mccullen, V. Ferrandiz-Mas, The effect of thermal cycling on the thermal and chemical stability of paraffin phase change materials (PCMs) composites, Mater. Struct. 58 (2025), https://doi.org/10.1617/s11527-024-02556-y.
[42] A. Arizzi, H. Viles, G. Cultrone, Experimental testing of the durability of lime-based mortars used for rendering historic buildings, Constr. Build. Mater. 28 (2012) 807–818, https://doi.org/10.1016/j.conbuildmat.2011.10.059.
[43] D.E.V. Madrid, C. Rodriguez-Navarro, C.W. Winardhi, N. De Belie, V. Cnudde, Controlling salt weathering of lime mortars by mixed-in additives: A multi-scale analysis, Constr. Build. Mater. 490 (2025), https://doi.org/10.1016/j.conbuildmat.2025.142603.
[44] L. Coppola, D. Coffetti, S. Lorenzi, Cement-Based Renders Manufactured with Phase-Change Materials: Applications and Feasibility, Adv. Mater. Sci. Eng. 2016 (2016), https://doi.org/10.1155/2016/7254823.
[45] A. Jayalath, R. San Nicolas, M. Sofi, R. Shanks, T. Ngo, L. Aye, P. Mendis, Properties of cementitious mortar and concrete containing micro-encapsulated phase change materials, Constr. Build. Mater. 120 (2016) 408–417, https://doi.org/10.1016/j.conbuildmat.2016.05.116.
[46] N.B. Srinivasaraonaik, L.P. Singh, S. Sinha, I. Tyagi, G. Mittal, Studies on thermal properties of microencapsulated eutectic phase change material incorporated different mortar mixes, Int. J. Energy Res. 45 (2021) 2488–2497, https://doi.org/10.1002/er.5943.
[47] R. Illampas, I. Rigopoulos, I. Ioannou, Influence of microencapsulated Phase Change Materials (PCMs) on the properties of polymer modified cementitious repair mortar, J. Build. Eng. 40 (2021), https://doi.org/10.1016/j.jobe.2021.102328.
[48] M. Kheradmand, M. Azenha, Assessment of the thermal performance of plastering mortars within controlled test cells, Clb-Mcs (2014), https://doi.org/10.13140/RG.2.1.1307.3760.
[49] Z. Pavlík, A. Trník, M. Keppert, M. Pavlíková, J. Zumár, R. Cerny, Experimental Investigation of the Properties of Lime-Based Plaster-Containing PCM for Enhancing the Heat-Storage Capacity of Building Envelopes, Int. J. Thermophys. 35 (2014) 767–782, https://doi.org/10.1007/s10765-013-1550-8.
[50] L. Ventolà, M. Vendrell, P. Giraldez, Newly-designed traditional lime mortar with a phase change material as an additive, Constr. Build. Mater. 47 (2013) 1210–1216, https://doi.org/10.1016/j.conbuildmat.2013.05.111.
[51] P.M. Mukadi, C. González-García, Time Series Analysis of Climatic Variables in Peninsular Spain. Trends and Forecasting Models for Data between 20th and 21st Centuries, Climate 9 (2021), https://doi.org/10.3390/cli9070119.
[52] European Committee for Standardization (CEN), EN 1367-1:2007 - Tests for thermal and weathering properties of aggregates - Part 1: Determination of resistance to freezing and thawing, 2008.
[53] European Committee for Standardization (CEN), EN 1367-2:2009 - Tests for thermal and weathering properties of aggregates - Part 2: Magnesium sulfate test, 2009.
[54] T. Hatakeyama, F.X. Quinn, Thermal analysis: Fundamentals and Applications to Polymer Science, 2nd ed., John Wiley & Sons, New York, 1995.
[55] P. Gabbott, Principles of Thermal Analysis and Calorimetry, 2008. ⟨https://doi.org/10.1039/9781847551764-00010⟩.
[56] B.A.C. David S. Moore, George P. McCabe, Introduction to the Practice of Statistics, 10th ed., W. H. Freeman and Company, New York, 2021.
[57] S.W. Wang, Z.B. Meng, Q.S. Zhao, T.F. Zhao, J. Jin, Z. Lu, Experimental study on the characteristics and resistance against the coupling effect of freeze-thaw and chloride salt erosion of sticky rice-lime composites modified with metakaolin and hemp fibers, Constr. Build. Mater. 416 (2024), https://doi.org/10.1016/j.conbuildmat.2024.135240.
[58] J.F. Gonzalez-Sanchez, B. Tasci, J.M. Fernandez, I. Navarro-Blasco, J.I. Alvarez, Combination of Polymeric Superplasticizers, Water Repellents and Pozzolanic Agents to Improve Air Lime-Based Grouts for Historic Masonry Repair, Polym. (Basel) 12 (2020) 887, https://doi.org/10.3390/polym12040887.
[59] W. Yue, B. Wang, Ceramic-added lime and cement mortars: A review of applications in building products, Sci. Prog. 107 (2024), https://doi.org/10.1177/00368504241266559.
[60] X.L. Wang, H.S. Shang, J.H. Zhou, L.L. Gu, Z.H. Xiao, X.Q. Wang, R.P. Wang, Enhancing Hydraulic Lime Mortar with Metakaolin: A Study on Improving Restoration Materials for Historic Buildings, Materials 17 (2024), https://doi.org/10.3390/ma17143548.
[61] A. Arizzi, G. Cultrone, Aerial lime-based mortars blended with a pozzolanic additive and different admixtures: A mineralogical, textural and physical-mechanical study, Constr. Build. Mater. 31 (2012) 135–143, https://doi.org/10.1016/j.conbuildmat.2011.12.069.
[62] M. Mahedi, B. Cetin, K.S. Cetin, Freeze-thaw performance of phase change material (PCM) incorporated pavement subgrade soil, Constr. Build. Mater. 202 (2019) 449–464, https://doi.org/10.1016/j.conbuildmat.2018.12.210.
[63] X.S. Yuan, B.M. Wang, P. Chen, T. Luo, Study on the Frost Resistance of Concrete Modified with Steel Balls Containing Phase Change Material (PCM), MATERIALS 14 (2021), https://doi.org/10.3390/ma14164497.
[64] Z.T. Zheng, W.B. Shen, S. Li, C. Li, P.J. Yin, M.J. Guan, J. Ha, Mechanical properties and Freeze-Thaw durability of concrete modified with microencapsulated phase change materials, Sci. Rep. 15 (2025), https://doi.org/10.1038/s41598-025-11371-6.
[65] B.P. Jelle, Accelerated climate ageing of building materials, components and structures in the laboratory, J. Mater. Sci. 47 (2012) 6475–6496, https://doi.org/10.1007/s10853-012-6349-7.
[66] C.C. Zhang, J.L. Li, M. Yu, Y. Lu, S.Z. Liu, Mechanism and Performance Control Methods of Sulfate Attack on Concrete: A Review, Materials 17 (2024), https://doi.org/10.3390/ma17194836.
[67] A.S. Silva, A. Gameiro, J. Grilo, R. Veiga, A. Velosa, Long-term behavior of lime-metakaolin pastes at ambient temperature and humid curing condition, Appl. Clay Sci. 88–89 (2014) 49–55, https://doi.org/10.1016/j.clay.2013.12.016.
[68] K. Van Balen, Carbonation reaction of lime, kinetics at ambient temperature, Cem. Concr. Res. 35 (2005) 647–657, https://doi.org/10.1016/j.cemconres.2004.06.020.
[69] UN Environment Programme, Global Status Report for Building and Construction - Towards a zero-emissions, efficient and resilient buildings and construction sector., 2019.
[70] J.I. Alvarez, R. Veiga, S. Martínez-Ramírez, M. Secco, P. Faria, P.N. Maravelaki, M. Ramesh, I. Papayianni, J. Válek, RILEM TC 277-LHS report: a review on the mechanisms of setting and hardening of lime-based binding systems, Mater. Struct. /Mater. Et. Constr. 54 (2021), https://doi.org/10.1617/s11527-021-01648-3.
[71] R.M. Lawrence, T.J. Mays, S.P. Rigby, P. Walker, D. D'Ayala, Effects of carbonation on the pore structure of non-hydraulic lime mortars, Cem. Concr. Res. 37 (2007) 1059–1069, https://doi.org/10.1016/j.cemconres.2007.04.011.

[72] M. Arandigoyen, B. Bicer-Simsir, J.I. Alvarez, D.A. Lange, Variation of microstructure with carbonation in lime and blended pastes, Appl. Surf. Sci. 252 (2006) 7562–7571, https://doi.org/10.1016/j.apsusc.2005.09.007.
[73] B.A. Silva, A.P.F. Pinto, A. Gomes, A. Candeias, Effects of natural and accelerated carbonation on the properties of lime-based materials, J. CO2 Util. 49 (2021), https://doi.org/10.1016/j.jcou.2021.101552.
[74] E. Aggelakopoulou, A. Bakolas, A. Moropoulou, Properties of lime-metakolin mortars for the restoration of historic masonries, Appl. Clay Sci. 53 (2011) 15–19, https://doi.org/10.1016/j.clay.2011.04.005.
[75] Y. Chen, P. Liu, Z.W. Yu, Effects of Environmental Factors on Concrete Carbonation Depth and Compressive Strength, Materials 11 (2018), https://doi.org/10.3390/ma11112167.
[76] C. Thiel, J. Kratzer, B. Grimm, T. Kraenkel, C. Gehlen, Effect of Internal Moisture and Outer Relative Humidity on Concrete Carbonation, CIVILENG 3 (2022) 1039–1052, https://doi.org/10.3390/civileng3040058.
[77] R.M. Espinosa-Marzal, G.W. Scherer, Impact of in-pore salt crystallization on transport properties, Environ. Earth Sci. 69 (2013) 2657–2669, https://doi.org/10.1007/s12665-012-2087-z.
[78] J. Todorovic, H. Janssen, The impact of salt pore clogging on the hygric properties of bricks, Constr. Build. Mater. 164 (2018) 850–863, https://doi.org/10.1016/j.conbuildmat.2017.12.210.
[79] A. Arizzi, J. Martínez-Martínez, G. Cultrone, D. Benavente, Mechanical evolution of lime mortars during the carbonation process. In: Key Eng. Mater, Trans Tech Publications Ltd, 2011, pp. 483–486, https://doi.org/10.4028/www.scientific.net/KEM.465.483.
[80] A. Török, B. Szemerey-Kiss, Freeze-thaw durability of repair mortars and porous limestone: compatibility issues, Prog. Earth Planet. Sci. 6 (2019), https://doi.org/10.1186/s40645-019-0282-1.